ELSEVIER

Applied Acoustics 59 (2000) 19–66

applied acoustics

www.elsevier.com/locate/apacoust

Scattering of a spherical wave by a thin hard barrier on a reflecting plane

D. Ouis*

Department of Engineering Acoustics, Lund Institute of Technology, PO Box 118, S-221 00, Lund, Sweden

Received 25 July 1997; received in revised form 2 February 1999; accepted 10 March 1999

Abstract

This paper is concerned with studying the problem of scattering of a spherical wave by a thin hard barrier on a hard plane. This problem is relevant to investigating the effect on the early part of the sound field of a large room, when a simple, thin and hard strip-like element is set horizontally on a side wall. This scattering element may be a sound reinforcing reflector or an idealisation of a side balcony. Three different calculation models based on ray acoustic concepts and on solutions to the problem of diffraction by a half plane are dealt with and compared to each other. For the case of the half plane, one of the models, the Biot–Tolstoy theory of diffraction, is a treatment in the time domain whereas the two other ones are approximate and give solutions in the frequency domain (one of them is the Geometrical Theory of Diffraction). The expression of the diffracted field in the time domain approach is exact but quite complicated so that, it has not been possible to give its Fourier transform in an exact form. In an earlier publication on this subject, the problem is overcome by making a simple analytical approximation of the early part the diffracted field, and then, adding to its exact Fourier transform the Digital Fourier Transform of the remaining part of the diffracted field. In this paper, an improvement is given to the expression of this early part of the diffracted field and it is shown that for both the time and the frequency domains, this new form is accurate enough for most engineering purposes. Moreover, the frequency form of this latter has a very simple expression. As one is interested in covering as large a low frequency range as possible, multiple diffraction is also implemented in each model to take into account the finite width of the barrier on the plane. Some experimental results are presented also supporting the theoretical predictions quite favourably.

Keywords: Scattering; Thin barrier; Biot–Tolstoy diffraction theory; Frequency domain; GTD; Multiple diffraction

* Tel.: +46-46-222-7403; fax: +46-46-222-4420.
E-mail address: djamel.ouis@kstr.lth.se (D. Ouis)

0003-682X/00/$ - see front matter
PII: S0003-682X(99)00017-1

1. Introduction

The problem of scattering by a thin strip has been studied for a long time. Since the work of Fresnel, who was the first to be able to give an accurate description of the diffraction by straight edges, many investigators have contributed to the elaboration of various solutions to the problem of wave diffraction by screens in the shape of strips. In fact, the problem of the strip has often been tied to that of the half plane, not only because the strip geometry is the most simple one in terms of diffraction after that of the half plane, but also because many of the solutions to the strip problem are formulated in terms of two half planes in mutual interaction. The equivalence of the solutions to the complementary problems of the strip and of the slit in a screen is made possible through the application of the important principle of Babinet. However, despite numerous efforts, no one has yet been able to present an elegant closed form solution to the strip problem like the ones found for the case of the half plane [1]. Moreover, most of these solutions treat the case of plane or cylindrical wave incidence thus making the problem into to a two dimensional one. Often, the more general case of spherical wave incidence has been approached only by approximate methods.

In the next section of this paper, the important results of the Biot–Tolstoy theory, subsequently referred to as the B–T theory, relevant to the case of the half plane are introduced. Medwin's first approximation of the diffracted field and its new improvement are then compared with numerical calculations. Section 3 considers the Geometrical Theory of Diffraction (GTD), which is based on geometrical optics assumptions. Consequently, it offers a high frequency approach. To extend it to lower frequencies, a new multiple diffraction algorithm, is added to the single diffraction formulation. A third approach to the problem of the wedge, also in the frequency domain, is that elaborated by Hadden and Pierce, henceforth identified as H–P model. The double and triple diffraction results for the barrier on the plane are compared to the previous approaches. Some experiments are also reported with some discussions on the possibilities for room acoustics applications. In the literature, there is sometimes some ambiguity regarding the expressions "diffraction" and "scattering". To avoid the risk of possible confusion, "diffraction" is used to describe the emanation of a wave from the sharp edge of an obstacle whenever a wave is incident upon it, whereas "scattering" is devoted to the contribution to the total field due to the extra presence of the obstacle.

2. The Biot–Tolstoy diffraction theory

Biot and Tolstoy presented the solution to the problem of diffraction of a pulse wave by an infinite fluid wedge with rigid boundaries more than 40 years ago [2]. This solution is based on geometrical optics constructions, though valid for all frequencies. As well as the geometrical components of the field, an observer receives a wave diffracted by the sharp edge of the wedge (Fig. 1).

The amplitude of the diffracted wave, which has further been elaborated by Medwin for the interesting case of a spherical Dirac pulse, may be expressed in an

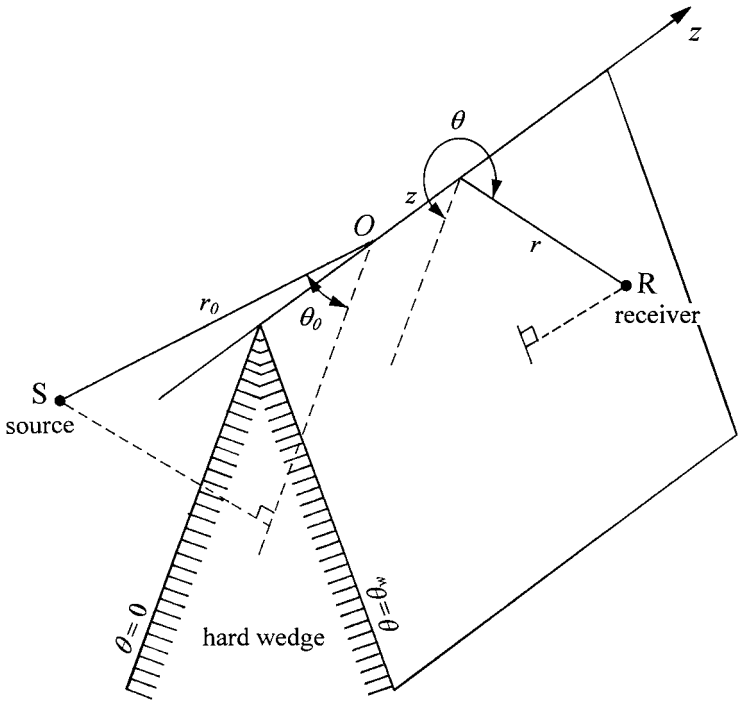

Fig. 1. Geometry for the problem of diffraction of a spherical wave by a hard wedge of exterior angle θ_W.

explicit closed form using rather simple mathematics. An important motivation for the use of transient waves in acoustical studies is the importance of the impulse response for extracting useful information about the system under investigation. Another reason is that it is quite common to study noise barrier performance at the scale model level. At this early stage of the experimental investigation, the use of short excitation pulses is often preferable due to the small sizes of anechoic spaces, and also because usually mathematical models are developed for the case of ideally infinite geometries, a fact that is surely not always true in reality.

Consider the geometry defined in Fig. 1. The wedge is composed of the two half planes at $\theta = 0$ and $\theta = \theta_W$ (for the half plane $\theta_W = 2\phi$). The sound source S and the observation point R have, respectively, for co-ordinates in the cylindrical system $(r_0, \theta_0, 0)$ and (r, θ, z).

If S radiates a delta function of pressure u_δ in the fluid of density ρ (air in our case),

$$u_\delta = \frac{\rho S}{4\pi R}\delta\left(t - \frac{R}{c}\right) \tag{1}$$

where S is the strength of the source, c the velocity of sound propagation and δ the Dirac delta function, then according to the B–T theory, the diffracted wave due to the tip of the wedge with the pressure $u_d(t)$ appears at a time τ_0:

$$\tau_0 = \left[(r + r_0)^2 + z^2\right]^{1/2}/c \tag{2}$$

after the source has emitted its spherically divergent pulse. τ_0 is called the least time over the wedge and is the travel time made by the wave in its shortest way from the point source to the field point via the crest line of the wedge. A practical consequence of this is the well known fact that the sharp straight edge of a metallic sheet presents a bright portion when illuminated by a small light source and observed from within the shadowed side. The expression of the diffracted field $u_d(t)$ may be considered as [3]:

$$u_d(t) = \frac{-S\rho c}{4\pi\theta_W}\{\beta\}\frac{\exp(-vy)}{rr_0\sinh(y)} \tag{3}$$

where:

$$y = \operatorname{arccosh}\frac{c^2t^2 - \left(r^2 + r_0^2 + z^2\right)}{2rr_0} \tag{4}$$

and:

$$\{\beta\} = \frac{\sin[v(\pi \pm \theta \pm \theta_0)]}{1 - 2\exp(-vy)\cos[v(\pi + \theta + \theta_0)] + \exp(-2vy)}; \quad v = \pi/\theta_W \tag{5}$$

Actually, the curly bracket $\{\beta\}$ is the sum of four terms resulting from the four possible combinations of the signs in $(\pi \pm \theta \pm \theta_0)$, and v is the wedge index and which takes the value $1/2$ for the case of the half plane.

Eq. (3) is developed in Appendix A for the important case of the half plane and for $z = 0$. The final result is given by:

$$u_d(t) = \frac{-S\rho}{4\pi^2 c}\sqrt{\frac{t_+^2 - t_-^2}{t^2 - t_+^2}}\left\{\frac{\cos[(\theta \pm \theta_0)/2]}{t^2 - t_+^2 + \left(t_+^2 - t_-^2\right)\cos^2[(\theta \pm \theta_0)/2]}\right\}_+ \tag{6}$$

where in this case $t_+ = \tau_0 = (r + r_0)/c$ and $t_- = (r - r_0)/c$. For writing convenience, the symbol $\{\ \}_+$ stands for the sum of two terms.

To see what happens in the frequency domain, the Fourier transform of $u_d(t)$ is needed:

$$u_d(f) = FT[u_d(t)] = \int_{\tau_0}^{\infty} u_d(t)\mathrm{e}^{j\omega t}\mathrm{d}t \tag{7}$$

Evaluating $u_d(f)$ exactly, if possible at all, is very cumbersome, and approximations are necessary for every particular case [4]. If, one notices, from Eq. (6), that the pressure near the least time τ_0 represents the main part of the energy [3,4], then for $\tau = t - \tau_0 << \tau_o$:

$$u_{di}(\tau) = -\frac{S\rho}{4\pi^2 c}\frac{1}{\sqrt{2t_+\left(t_+^2 - t_-^2\right)}}\left\{\frac{1}{\cos[(\theta \pm \theta_0)/2]}\right\}_+ \frac{1}{\sqrt{\tau}} \tag{8}$$

i.e.:

$$u_{di}(\tau) \sim \frac{1}{\sqrt{\tau}} \tag{9}$$

a form which is better suited for calculations. The Fourier transform of this last expression is given as:

$$FT[u_{di}(\tau)] = u_{di}(f) = \int_0^\infty u_{di}(t - \tau_0)\mathrm{e}^{i\omega t}\mathrm{d}t \tag{10}$$

and with the change of variable $\tau = t - \tau_0$ one obtains

$$u_{di}(f) \sim \mathrm{e}^{i\omega\tau_0}\int_0^\infty u_{di}(\tau)\mathrm{e}^{i\omega\tau}\mathrm{d}\tau \tag{11}$$

which, when decomposed into two (cos and sin) Fourier transforms leads to [5]:

$$u_{di}(f) = \frac{-S\rho}{4\pi^2 c}\frac{1}{\sqrt{2t_+\left(t_+^2 - t_-^2\right)}}\left\{\frac{1}{\cos[(\theta \pm \theta_0)/2]}\right\}_+ \mathrm{e}^{i\omega\tau_0}\frac{1+i}{2\sqrt{f}} \tag{12}$$

This result enables an approximation of the total Fourier transform of Eq. (6) by the sum of Eq. (12) and a digital Fourier transform (DFT) of the rest of the time signal [3], i.e.:

$$u_d(f) = u_{di}(f) + DFT[\Delta u_d(\tau)]; \qquad \Delta u_d(\tau) = u_d(t) - u_{di}(\tau) \tag{13}$$

$\Delta u_d(\tau)$ is sampled at a frequency $1/\Delta T$ over a time length T which is for instance chosen such that $\Delta u_d(T)$ is less than 5% of the maximum value of $\Delta u_d(\tau)$, and ΔT is given a value such that the highest desired frequency component $f_{\max}$ is accounted for by the FFT analysis i.e.:

$$\frac{1}{2\Delta T} > f_{\max} \tag{14}$$

To smooth the data, the late part of $\Delta u_d(\tau)$ may be tapered by a half cosine window extending for instance over a length of $T/10$ before applying the DFT [6]. With the same calculation strategy in mind, a new approximation of the initial short time range diffracted field is suggested in this paper. Indeed, Eq. (6) may be better approached by:

$$u_{di,\mathrm{new}}(\tau) = \frac{-S\rho}{4\pi^2 c}\sqrt{\frac{t_+^2 - t_-^2}{2t_+}}\frac{1}{2t_+}\frac{1}{\sqrt{\tau}}\left\{\frac{\cos[(\theta \pm \theta_0)/2]}{\tau + \dfrac{t_+^2 - t_-^2}{2t_+}\cos^2[(\theta \pm \theta_0)/2]}\right\}_+ \tag{15}$$

The Fourier transform of (15) leads to the sum of two terms of the form:

$$\mathrm{e}^{i\omega\tau_0}\int_0^\infty \frac{\mathrm{e}^{i\omega\tau}}{\sqrt{\tau}(\tau + a)}\,\mathrm{d}\tau \tag{16}$$

which when performed yields [7]:

$$u_{di,\mathrm{new}}(f) = \frac{-S\rho}{4\pi^2 c}\frac{\pi \mathrm{e}^{i\omega\tau_0}}{2t_+}\left\{\mathrm{sgn}(\pi \mp \theta_0 - \theta)\mathrm{e}^{-i\omega a_\pm}\mathrm{erfc}\left(\sqrt{-i\omega a_\pm}\right)\right\}_+ \tag{17}$$

where:

$$a_\pm = \left(t_+^2 - t_-^2\right)\cos^2[(\theta \pm \theta_0)/2]/(2t_+) \tag{18}$$

and erfc is the complementary error function and which is examined in Appendix B for the case of a complex argument with real and imaginary parts of equal magnitude.

The performances of these two approximations were compared to a numerical Fourier transform calculation of Eq. (6) using the NAG software package [8]. Keeping the source position constant and varying the frequency of the spherical wave gives the results in Fig. 2 for two different receiver positions.

One already sees that over a wide frequency range, the new approximation of the diffracted field follows the numerical integration almost perfectly so that for most engineering purposes, an extra consideration of the DFT of the remaining part of the diffraction field seems unnecessary. A further observation is that the discrepancies between the two approximations may be quite appreciable especially in the regions of space near the geometrical boundaries [see Fig. 2(a)], and that away from these regions this difference shrinks noticeably. This is better illustrated in Fig. 3 where for a constant frequency and for a fixed position of the point source, the observation point follows a circle around the edge of the half plane.

Two important properties of the diffracted field are, first, its symmetrical character about the half plane and second, that its amplitude is of the same order of magnitude as that of the incident or reflected field at the respective geometrical boundaries.

3. The geometrical theory of diffraction

In the GTD approach, diffraction is considered as a local phenomenon, i.e. it is a correction to geometrical optics due to the presence of scattering objects or

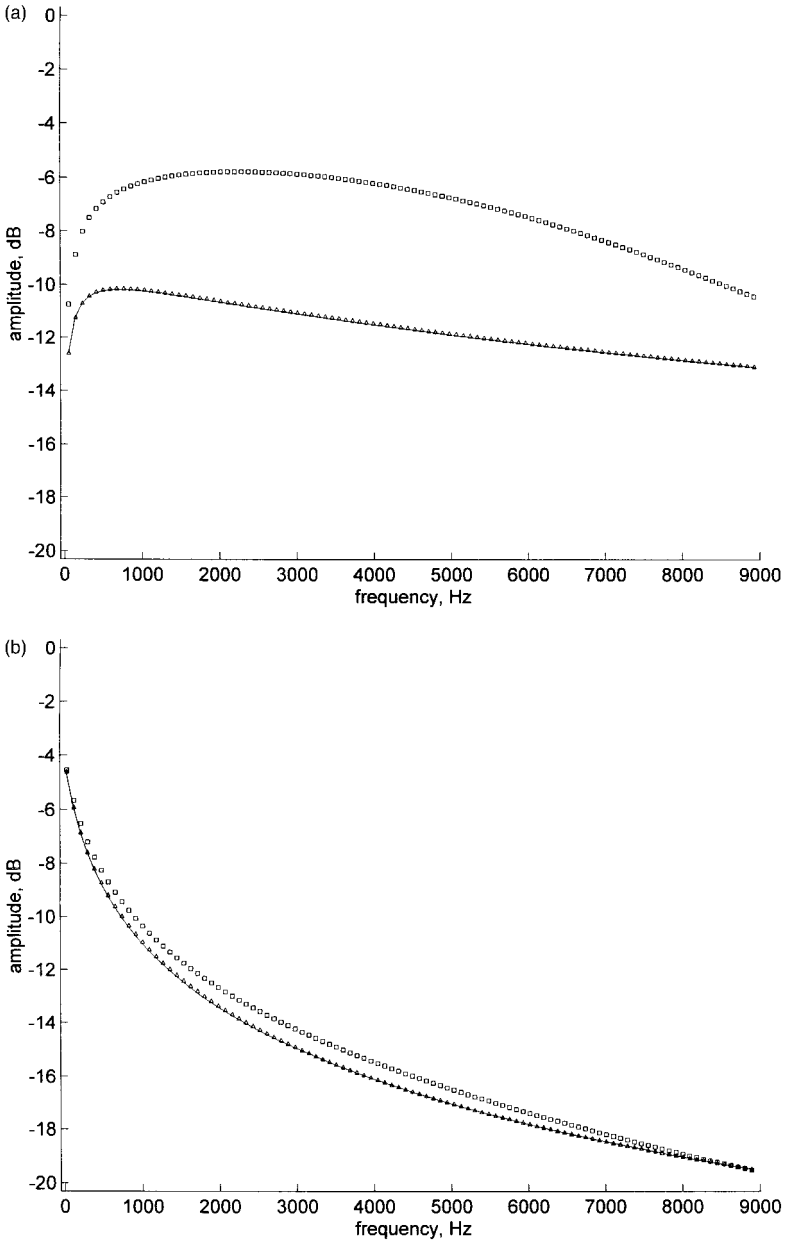

Fig. 2. Amplitude in dB of the diffracted field by a half plane normalised to the free field at $r + r_0$.—: numerical Fourier transform of Eq. (6) = □: Eq. (12) Δ: Eq. (17). $r_0 = 1$ m, $r = 0.5$ m, $\theta_0 = 60°$. (a) $\theta = 130°$; (b) $\theta = 280°$.

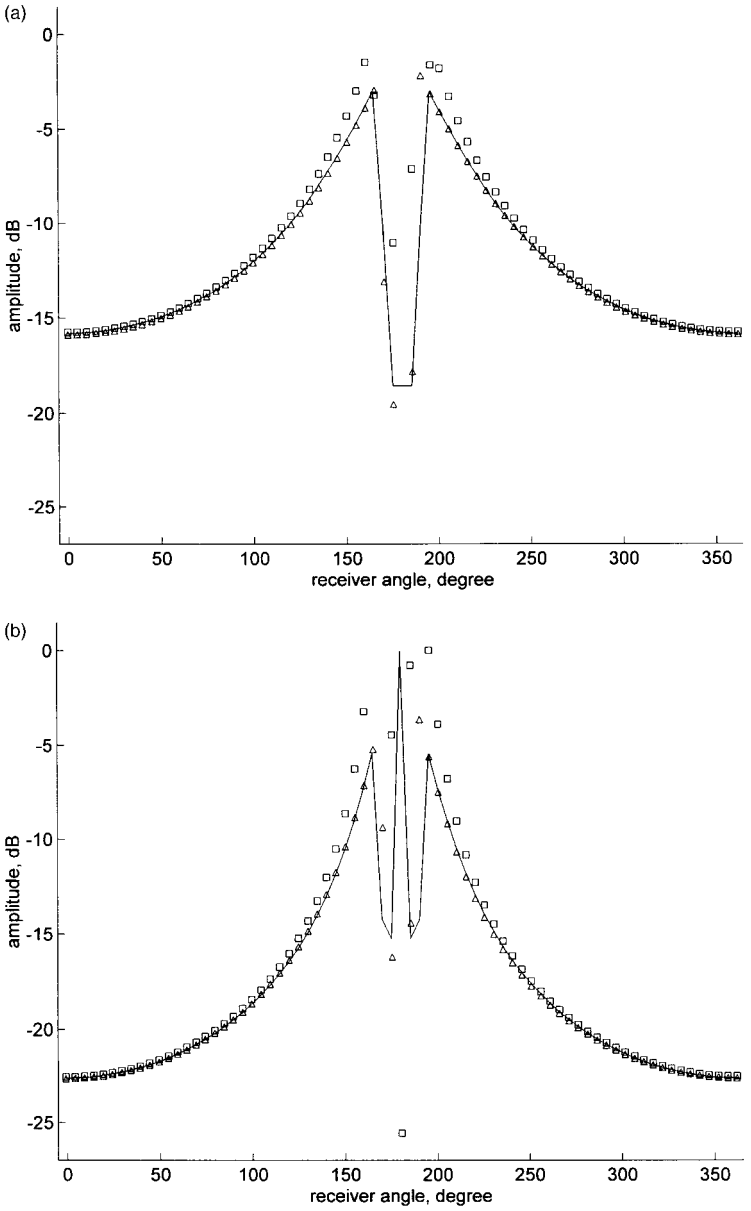

Fig. 3. Same legend as for Fig. 2, except that $\theta_0 = 10°$ and the receiver is moving on a circle around the edge of the half plane. (a); f = 1000 Hz (b); f = 5000 Hz.

diffracting edges. In wave theory, ray considerations still play a significant role and a logical extension is to apply this concept to treat of diffraction; The Geometrical Theory of Diffraction (GTD) is devoted to such a role. Good and extensive accounts of the GTD are available in Refs. [9] and [10].

The GTD postulates that the field at any point is due to the possible arrival of three kinds of rays: direct, reflected and diffracted. The two first contributions occur, respectively, whenever the observer "sees" the source and its image(s) through the diffracting surface while the third kind of rays emerge whenever one or both of the rays of the first kind hit upon an edge [11].

The field u_i on a ray is assumed to be given by:

$$u_i(R) = A(R)\mathrm{e}^{-ikr(R)} \tag{19}$$

where $A(R)$ is the amplitude, $kr(R)$ is the phase along the ray at R and k is the wavenumber. The difference in phase between two points R and R′ on the same ray is given by the product of the wavenumber k times the length difference between the two points:

$$kr(R') = kr(R) + kl(R, R') \tag{20}$$

and for homogeneous media the rays are straight lines so that $l(R, R')$ is just the distance between R and R'. The GTD stipulates furthermore that a ray which hits an edge gives rise to a cone of diffracted rays. The apex of this latter which is the intersection point of the incident ray with the edge, is called the diffraction point, Q (see left-hand side of Fig. 4), and the half angle of the cone is equal to the angle made by the incident ray and the tangent to the edge at Q. This is Keller's law of edge diffraction.

An especially important case is when the incident ray falls normally on the edge. The cone then degenerates to a plane perpendicular to the edge (see right-hand side of Fig. 4).

If a diffracted ray hits an edge, then it gives rise to a doubly diffracted ray and if this latter in its turn hits another edge, it generates a diffracted ray of third order and so on.

Considering the diffraction geometry shown on the left hand side of Fig. 4, the field on a diffracted ray at a point R, a distance r from Q, is given by:

$$u_d(R) = u_i(Q)A(r', r)D_{s,h}\mathrm{e}^{-ikr} \tag{21}$$

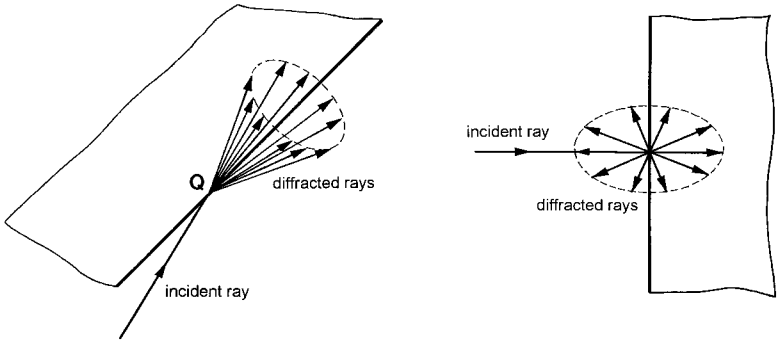

Fig. 4. Illustration of the cone of diffracted rays. Left: arbitrary incidence; right: normal incidence.

where $u_i(Q)$ is the incident field at Q, $A(r', r)$ a coefficient depending on the characteristics of the source of the primary rays, r' being the distance from the source to Q in case if it is cylindrical or spherical. $D_{s,h}$ is another coefficient depending on the angles of the incident and diffracted rays and on the diffracting screen, s and h standing respectively for the soft and hard cases. $D_{s,h}$ is determined from comparison with the exact solution for the plane wave diffraction by a half plane [12]. At quite high frequencies, the geometrical optics components may be extracted from the expression of the total field. An examination of the field in the shadow zone reveals that a wave of a cylindrical type seems to emanate from the edge of the half plane. It is the expression of this field that enables the identification of the value of $D_{s,h}$ in Eq. (21). However, as formulated in its original form, and for an arbitrary oblique incidence of the plane wave on the half plane with an angle β, the GTD assigns to $D_{s,h}$ the value:

$$D_{s,h} = -\frac{e^{-i\pi/4}}{2\sqrt{2\pi k}\sin\beta}\left[\sec\left(\frac{\theta-\alpha}{2}\right) \pm \csc\left(\frac{\theta+\alpha}{2}\right)\right]. \tag{22}$$

This fails to predict the correct value of the diffracted field near to the geometrical boundaries (i.e. at $\theta = \pi \pm \alpha$). This has encouraged the elaboration of several refinements to this theory in particular the Uniform GTD (UTD) has been shown to be relatively simple and powerful in many practical situations [13]. According to this, after defining the new angles $\varphi = 3\pi/2 - \alpha$ and $\varphi' = 3\pi/2 - \theta$, the coefficients A and $D_{s,h}$ in Eq. (21) are given by:

$$A(r', r) = \begin{cases} \dfrac{1}{\sqrt{r}} & \text{for plane and cylindrical wave incidence} \\ \sqrt{\dfrac{r'}{r(r'+r)}} & \text{for spherical wave incidence} \end{cases} \tag{23}$$

and:

$$D_{s,h} = \frac{-e^{-i\pi/4}}{\sin\beta}\sqrt{\frac{L}{\pi}} \left\{ \begin{array}{l} f(kL, \varphi' - \varphi)\exp\left[i2kL\cos^2\left(\dfrac{\varphi'-\varphi}{2}\right)\right]\mathrm{sgn}(\pi+\varphi-\varphi')\mp \\ \mp f(kL, \varphi+\varphi')\exp\left[i2kL\cos^2\left(\dfrac{\varphi+\varphi'}{2}\right)\right]\mathrm{sgn}(\pi-\varphi'-\varphi) \end{array} \right\} \tag{24}$$

where L is a distance parameter given by:

$$L = \begin{cases} r\sin^2\beta & \text{for plane wave incidence} \\ \dfrac{rr'}{r+r'} & \text{for cylindrical wave incidence} \\ \dfrac{rr'}{r+r'}\sin^2\beta & \text{for spherical wave incidence} \end{cases} \tag{25}$$

f is a form of Fresnel integral:

$$f(\alpha, \gamma) = \int_{\sqrt{2\alpha}|\cos(\gamma/2)|}^{\infty} e^{-i\tau^2} d\tau \tag{26}$$

and sgn is the signum function:

$$\mathrm{sgn}(x) = \begin{cases} +1 & \text{for } x > 0 \\ 0 & \text{for } x = 0 \\ -1 & \text{for } x < 0 \end{cases} \tag{27}$$

This new expression of the diffracted field ensures that the total field is continuous throughout all space because the discontinuities in the geometrical field are exactly compensated by those in the diffracted field.

4. A Green's function solution for the wedge problem

The Green's function solution for the diffraction of a spherical wave by a hard wedge is inspired by classical theory [14]. Approximations are necessary as a result of numerical difficulties faced in attempting to give closed form solutions. These have been presented by Hadden and Pierce [15,16] for the cases where the receiver is situated in the far-field or at the geometrical shadow boundaries. Related work has reported agreement with carefully-mounted experiments [17]. More recently, this model has been applied to diffraction of acoustic impulses [18].

The solution to the Helmholtz equation satisfying the hard boundary conditions, $\partial u/\partial n = 0$ on the sides of the hard wedge $\theta = 0$ and $\theta = \theta_W$ (see Fig. 1) may be expressed as:

$$u = \sum_{i=1}^{4} [u(\xi_i) H(\pi - \xi_i) + u_d(\xi_i)] \tag{28}$$

where:

$$\xi_1 = |\theta_0 - \theta|; \quad \xi_2 = 2\theta_w - \xi_1; \quad \xi_4 = \theta + \theta_0; \quad \xi_3 = 2\theta_W - \xi_4 \tag{29a–d}$$

and $H(\alpha)$ is the Heaviside unit step function.

The first three terms of the field are found from pure geometrical considerations that is for $i = 1$, 3 and 4, $u(\xi_i)H(\pi - \xi_i)$ represent, respectively, the direct and the reflected waves from the sides $\theta = 0$ and $\theta = \theta_W$ of the wedge. ξ_2 being always greater than π, the term $u(\xi_2)H(\pi - \xi_2)$ is always zero and is written only for the tractability of the expression for the field. The $u(\xi_i)$ are supposed to be of the form e^{ikR_i}/R_i with:

$$R_i = \left[r^2 + r_0^2 + z^2 - 2rr_0 \cos \xi_i\right]^{1/2} \tag{30}$$

The sum on the left-hand side of the expression for the total field [Eq. (28)] $\left(\sum_{i=1}^{4} u_d(\xi_i)\right)$ may be interpreted as a diffracted wave. For each ξ_i, u_d is expressed as an integral of the form:

$$u_d(\xi_i) = -\frac{1}{\pi}\int_0^{\infty} u(\pi + iw)Q(w, v, \xi_i)\mathrm{d}w \tag{31}$$

where:

$$Q(w, v, \xi_i) = \frac{(v/2)\sin[v(\pi - \xi_i)]}{\cosh(vw) - \cos[v(\pi - \xi_i)]} \tag{32}$$

$v = \pi/\theta_w$ being the wedge index seen earlier, and $u(\pi + iw)$ is the previous e^{ikR}/R but now with ξ in Eq. (30) replaced by $(\pi + iw)$.

Because of the oscillatory character of the integral in (31), its direct numerical evaluation presents some difficulties, but some useful approximations for the most practical cases have been presented. Hence, a new form for the integral is presented with a new parameter A:

$$A(\xi_i) = (v/2)(-\theta_w - \pi + \xi_i) + \pi H(\pi - \xi_i) \tag{33}$$

and with this in mind the new expression of u_d reads then as:

$$u_d(\xi_i) = (-1/\pi)A(\xi_i)(\mathrm{e}^{ikL}/L)F_v(|A|, \alpha, \varepsilon) \tag{34}$$

in which:

$$F_v(|A|, \alpha, \varepsilon) = \int_0^1 I(q)\mathrm{d}q \tag{35}$$

$$a = krr_0/L; \quad \varepsilon = rr_0/L^2; \quad L = \left[(r + r_0)^2 + z^2\right]^{1/2} \tag{36}$$

$$I(q) = (L/R)\mathrm{e}^{ik(R-L)} \tag{37}$$

L, the least time path, is the shortest two segment distance from the point source to the field point via the edge, and is simply equal to the product of the least time τ_0 in Eq. (2) and the velocity of sound c.

Approximations of u_d for different values of A, α and ε are presented next. For the case at hand, the following results are obtained:

Where both the source and the receiver are far from the edge of the wedge, $\alpha = krr_0/L >> 1$ and $|A|$ is arbitrary, one has [15]:

$$Fv(|A|, \alpha, \varepsilon) \cong \frac{\pi}{\sqrt{2}}\frac{\sin|A|}{|A|}\frac{\mathrm{e}^{i\pi/4}}{\left[1 + (2\varepsilon + 1/2)\cos^2|A|/v^2\right]^{1/2}}A_D(P) \tag{38}$$

with:

$$A_D(p) = \frac{P}{\sqrt{\pi}} \int_0^{\infty} \frac{e^{-u^2}}{(\pi/2)P^2 + iu^2} du = f(P) - ig(P) \tag{39}$$

and:

$$P = \left(\frac{4\alpha}{\pi}\right)^{1/2} \frac{\cos|A|}{\left[v^2 + (2\varepsilon + 1/2)\cos^2|A|\right]^{1/2}} \tag{40}$$

$A_D(P)$ is expressed in terms of the Fresnel integrals and is detailed in Appendix C.

5. Model implementations

5.1. Single diffraction

Each of the three models previously presented has been used to predict the scattered field due to a spherical source in the presence of a large hard plane containing a vertical thin hard strip (see Fig. 5).

The thin hard strip of height h is perpendicular to the $x = 0$ plane and is parallel to the z axis. S is the point source with co-ordinates $(R_0, \varphi_0, 0)$ and R is the field point with co-ordinates $(R, \varphi, 0)$. S', R' and H' are the images through the plane of, respectively, S, R and the tip H(0,h,0) of the strip, and S″ is the image of S′ through the plane containing the strip. One is interested only in the space quadrant containing S, that is $0 \leqslant \varphi \leqslant \pi/2$. The total field at R is composed of:

- a direct wave, S–R
- a reflected wave S′-R, and

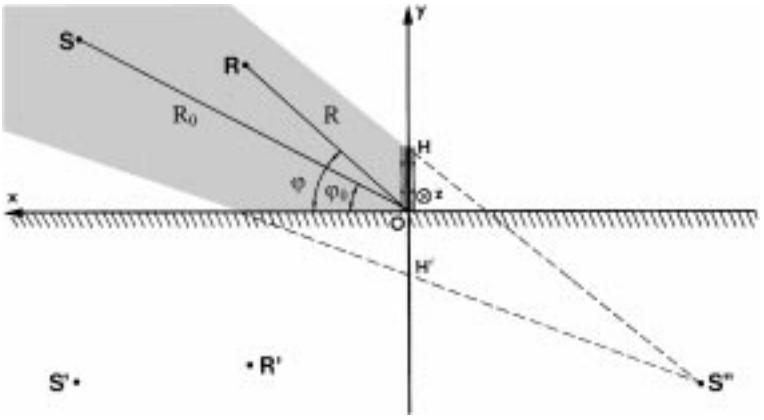

Fig. 5. The thin hard strip on the reflecting plane.

- a doubly reflected wave, S″-R, in the greyed zone and a diffracted field due to the edge of the strip and made of the following contributions:
- real source–edge–real point, SHR
- image source–edge–real point, S′HR
- real source–edge–image point, SHR′
- image source–edge–image point, S′HR′

The corner at the origin of co-ordinates 0 does not contribute to the diffraction. This can be confirmed theoretically by setting $\nu = 2/3$ in Eqs. (3) or (32), and has been verified experimentally quite a long ago for the case of electromagnetic waves [19].

5.2. Multiple diffraction

The diffracted rays emerging from the top of the barrier and propagating tangentially to it can give rise to second order diffracted rays. In fact, two rays propagating along the y axis from H to 0 ($\theta = 0$ and $\theta = 2\pi$ in Fig. 1), get reflected on the plane, return back to H (illustrated by arrows in Fig. 5) and thereby generate a new set of diffracted rays.

For the B–T theory, only the second order diffracted field is formulated. This is given in detail in Appendix D.

Using GTD, it is relatively easy to calculate the strength of the second order diffracted field and even to derive from it that of the higher order multiply diffracted ones. This is the result of the relatively simple expression for $D_{s,h}$ in Eq. (24), and is detailed in Appendix E.

The asymptotic double diffraction to the Green's function approach [20] has even been extended to a triple diffraction [21]. For details, see Appendix F.

6. Numerical results

The amplitude of the scattered field at some observation point is evaluated and presented in either of two ways; the frequency spectrum for a fixed combination of the positions of the point source and the field point, or alternatively, its angular variation, for a fixed frequency and fixed position of the source, but a varying position of the field point.

The calculations have been performed for $R_0 = 1$m, $R = 0.5$ m and $h = 0.1$ m, with different combinations of the pair of angles (φ_0, φ) (see Fig. 5).

6.1. The B–T theory

First, a comparison is made in the time domain between the evaluations of the scattered field, given by its exact expression, Eq. (6), and by both its short time approximations [Eq. (8)] and its new improvement [Eq. (15)]. This is shown in Fig. 6 for $(\varphi_0, \varphi) = (30^\circ, 60^\circ)$.

The relative field difference $|(u_d - u_{di})/u_d|$ is plotted for times after the least time. This is represented in Fig. 7 to compare the behaviour of the wakes of the diffracted field expressed by the crude first approximation [Eq. (8)] and its improvement [Eq. (15)]. One can conclude that the improved approximation agrees better with the exact expression for small values of ΔT (the difference between their predictions tends to zero). For longer times, the improved approximation attenuates faster.

The frequency domain of the scattered field, for the geometrical configuration of Fig. 7 includes the contribution of both the Fourier transform of the diffracted fields and that of the image source S′, and results in the curves in Fig. 8.

When one uses the improved approximation of the diffracted field, Eq. (17), and takes into consideration the double diffraction detailed in Appendix D, then one gets the curves of Fig. 9.

6.2. The GTD

The results of the calculations using the single diffraction and the multiple diffraction formulations detailed in Appendix E are illustrated in Fig. 10.

6.3. The Green's function approach

The results of calculations based on the Green's function approach are comparable to those of the improved approximation to the B–T theory [Eq. (17)] so it is not necessary to plot the same curves again. However, the improvements to the scattered

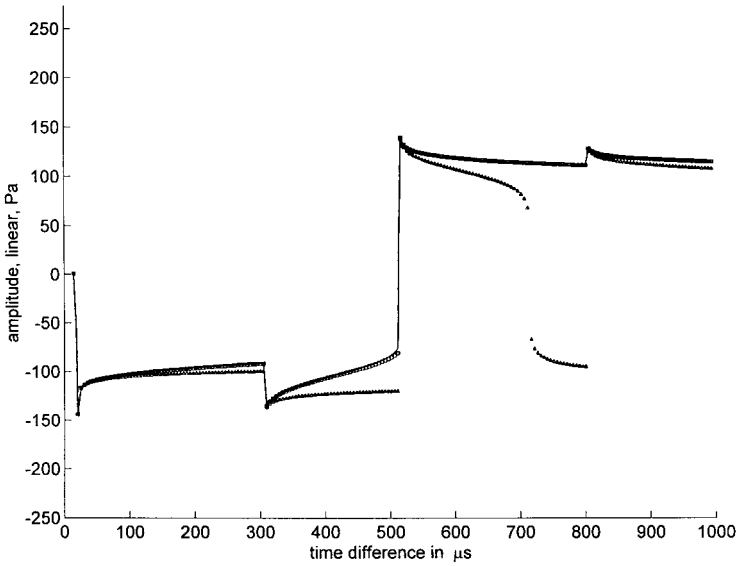

Fig. 6. The diffracted field due to the edge of the strip for $(\varphi_0, \varphi) = (30°,60°)$. —: exact after Eq. (6) ; Δ: Eq. (8) ; □: Eq. (15).

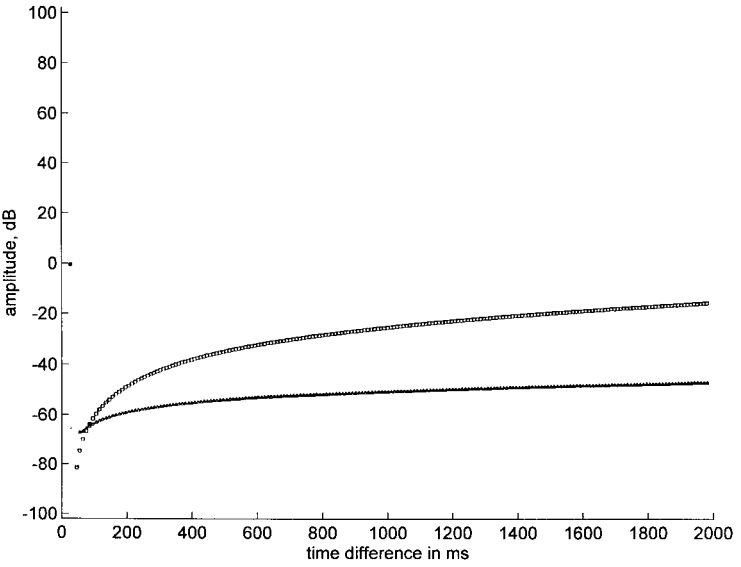

Fig. 7. Prediction of the field difference in dB relative to the exact solution [Eq. (6)] after 2 s from the shortest least path time for $(\varphi_0, \varphi) = (30°, 60°)$. Horizontal axis: time in ms; vertical axis: relative sound pressure, log. Δ: after Eq. (8); □: after Eq. (15).

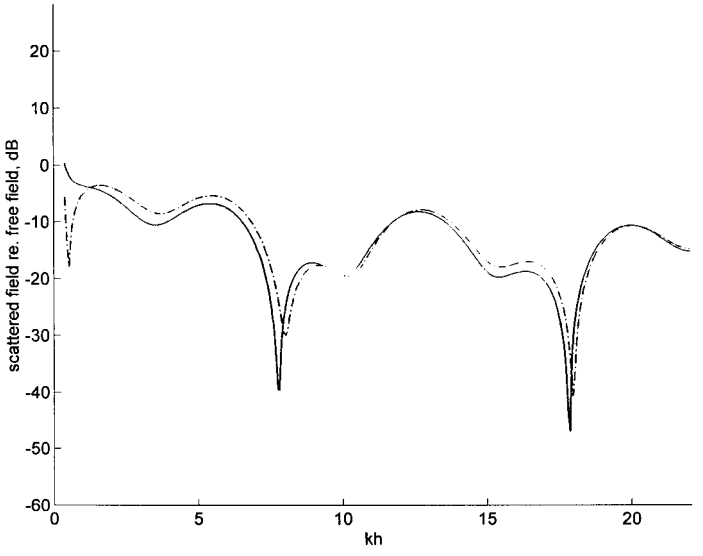

Fig. 8. The scattered field corresponding to Fig. 6 in the frequency domain. –·–·–: using Eq. (12); ——: using Eq. (17).

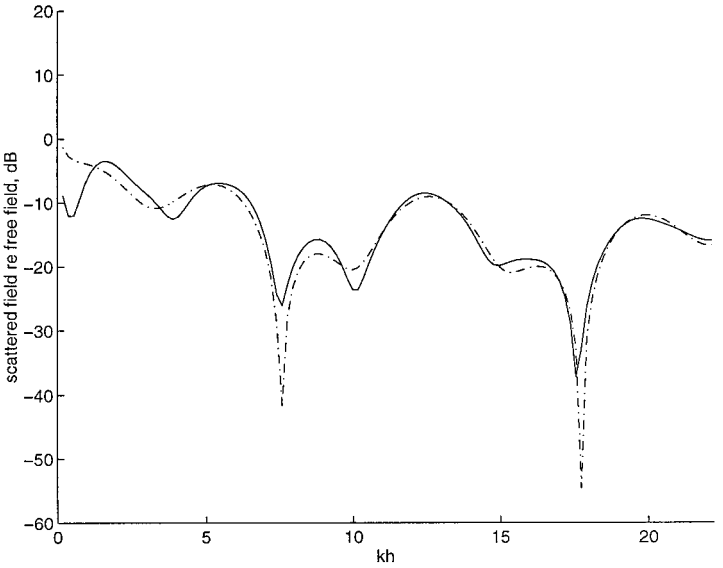

Fig. 9. As for Fig. 8 using Eq. (17). ·-·-·-: single diffraction; ——: single + double diffraction. Number of secondary sources NSS = 15.

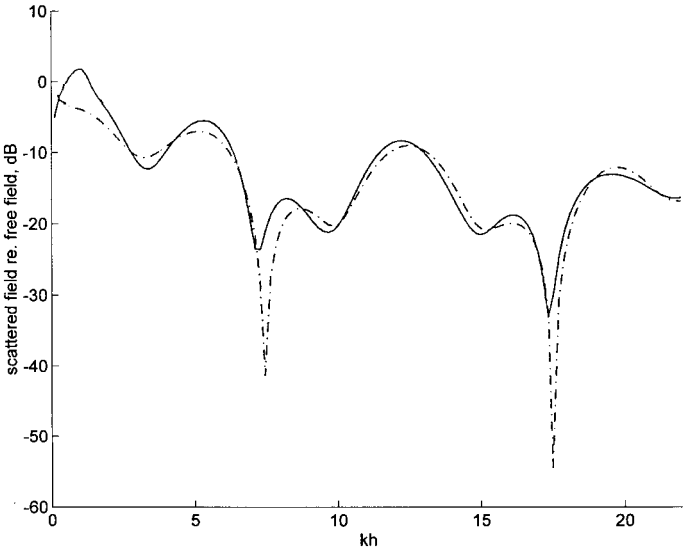

Fig. 10. Sound pressure level of the scattered field using the GTD re. free field in dB. $\varphi_0 = 30°$; $\varphi = 60°$. –·–·–: single diffraction; ——: multiple diffraction.

field that follow from the inclusion of multiple diffraction amount to less than about 0.5 dB for almost the whole frequency range of interest.

7. Experiment

7.1. Experimental configuration

The experiment was intended to be as simple as possible consistent with an overall crude check of the validity of the theoretical predictions. The experimental configuration is shown in Fig. 11.

The sound source was a high frequency driving unit Dynaudio D28-AF fed by an amplified square pulse of a short enough time duration to cover as wide a low frequency range as possible and, amplified to achieve a satisfactory signal to noise ratio. The shape of the pulse both in the time and frequency domains is shown in Fig. 12.

To avoid problems of calibration and also to give a better quantitative interpretation, the scattered field in the frequency domain was normalised to the free field pressure as measured for a distance source receiver equal to $R + R_0$ (see Fig. 5).

The measuring and triggering microphones shown in Fig. 11 were a pair of phase matched half inch B&K units of type 4165. The role of the triggering microphone was to position the signal recorded by the measuring microphone at a suitable time

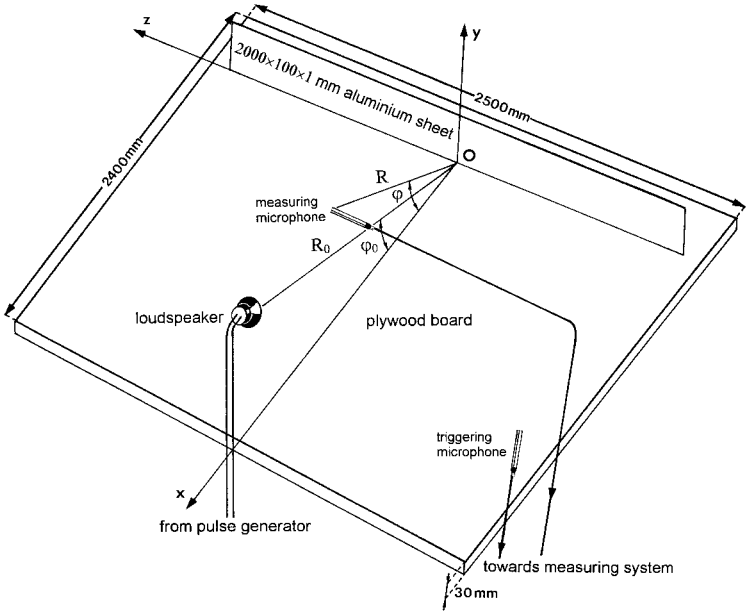

Fig. 11. Thin hard barrier set normally on a reflecting plane: experimental set-up.

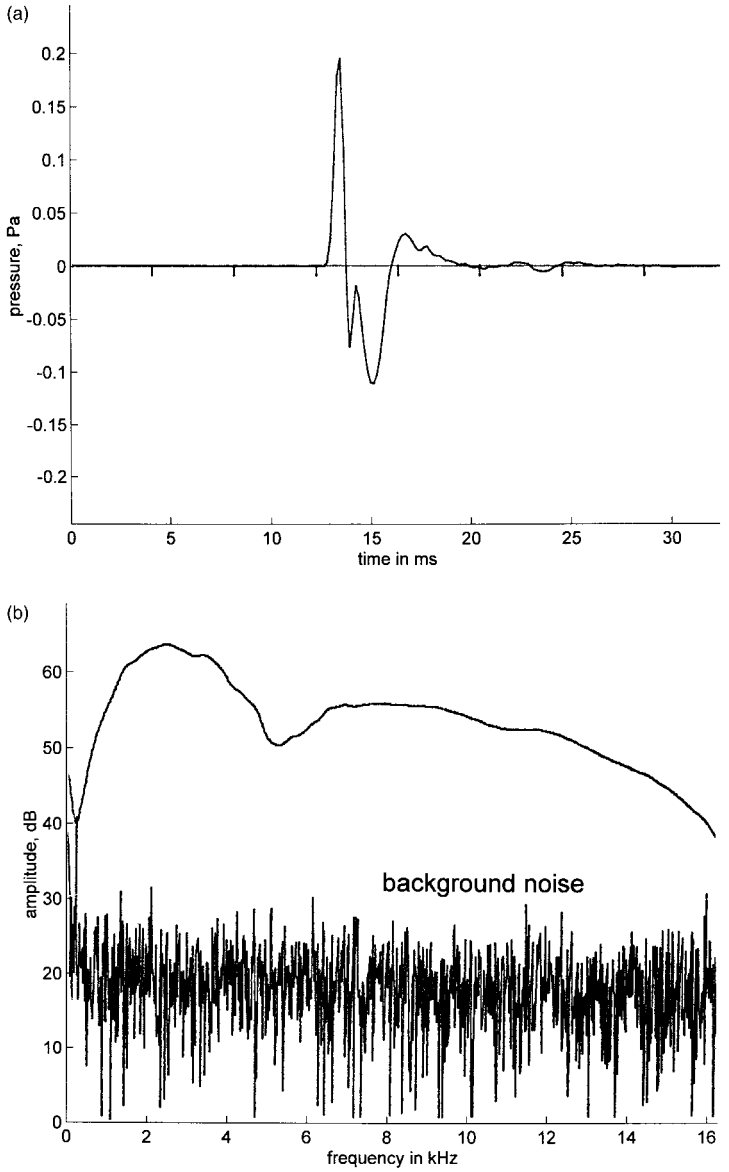

Fig. 12. The pulse signal: (a) in the time domain; (b) in the frequency domain.

delay in order to get an idea about the phase behaviour. The signals from these two microphones were picked up and processed by a computer aided test system (GENRAD 2515).

7.2. Experimental results

The numerical results as presented in sec. 6 show relatively good agreement between the three theoretical models. The measured scattered fields, for two different configurations of the source and the receiver positions, are compared to their theoretical predictions in Figs. 13 and 14.

The other experimental procedure was to fix the frequency and position of the sound source, and to revolve the field point along a quarter circle in the plane normal to the strip and containing the source. Fig. 15 shows polar plots for three different frequencies and for $\varphi_0 = 45°$:

8. Application to a horizontal barrier on a hard wall

This section attempts to predict the field scattered by a thin hard strip which is set horizontally on a hard wall. Such a set-up could be a simplified representation of some reflector or of a side balcony in an auditorium. It is informative to consider the strength of the different components of the edge diffracted field contributing to the field scattered by the barrier. As seen earlier, the field diffracted from the sharp straight edge of a half plane exhibits its strongest amplitude at the passage through the geometrical boundary zones. The diffracted field at a point revolving around the edge of a thin half plane is shown in Fig. 16 where the exact form, Eq. (6), has been used for the numerical calculations.

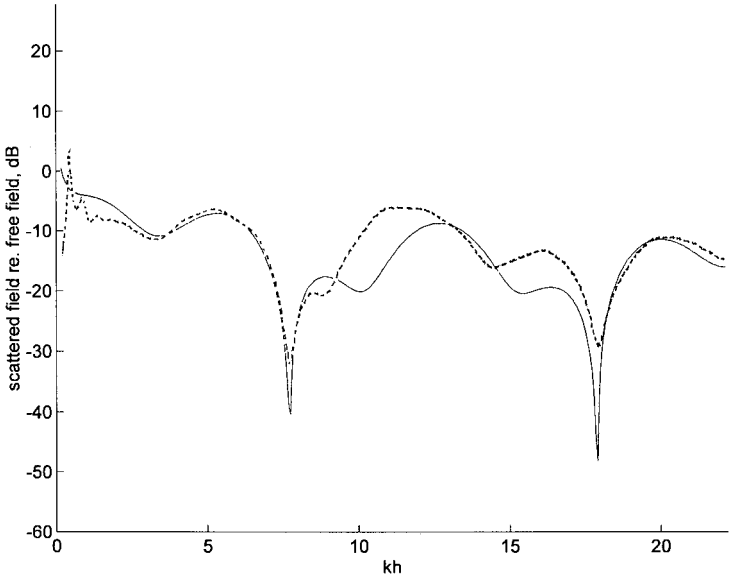

Fig. 13. Scattered field re. free field in dB. $(\varphi_0, \varphi) = (30°, 60°)$. ——: Theoretical; - - - : experimental.

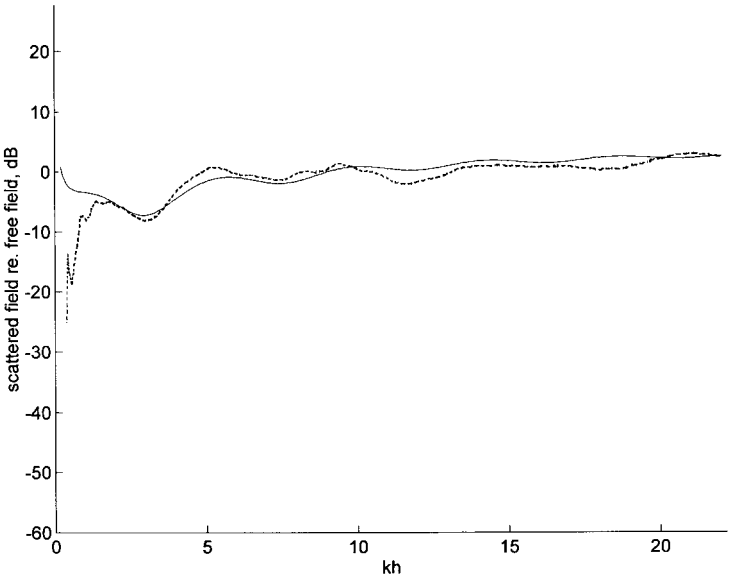

Fig. 14. As Fig. 13 but for $(\varphi_0, \varphi) = (45°, 45°)$.

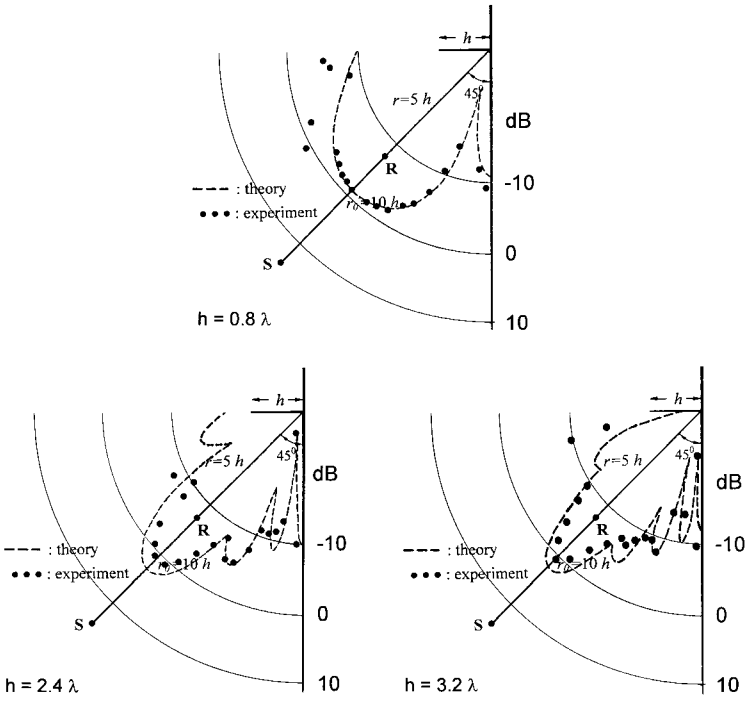

Fig. 15. Scattered field for $\varphi_0 = 45°$ and for different frequencies.

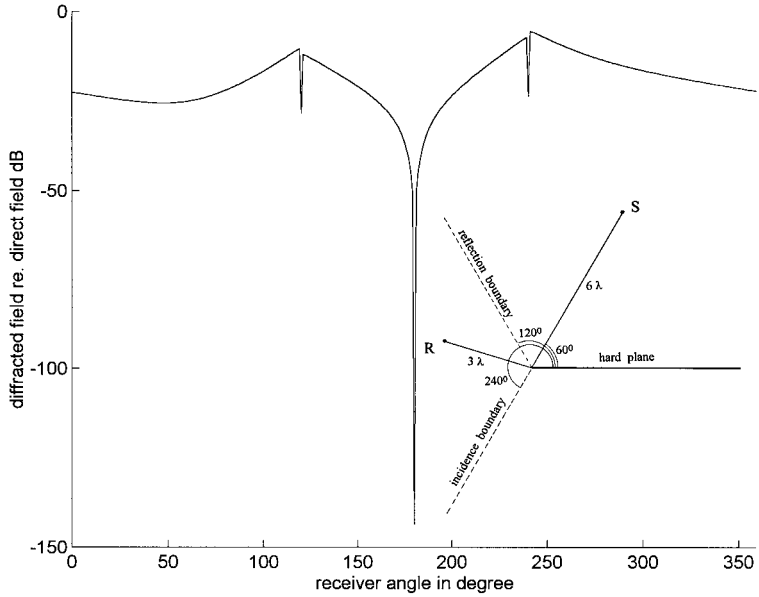

Fig. 16. Amplitude in dB of the diffracted field at a point moving around the edge of a half plane.

If the barrier is on a hard plane, the amplitude of the various diffraction components have the frequency spectra shown in Fig. 17. Note the quite marked strength of the SHR' component compared with the other three components. This is due to the proximity of the field point to one of the geometrical boundary zones. The diffraction component has an amplitude about half that of the double specularly reflected reflection, S″R, over almost the whole audio frequency range. The component SHR, which could be taken perhaps misleadingly as the only contribution to the totally diffracted field, has an amplitude about 50 dB less than that of the SHR component. Hence, when approximations are to be made, it is important to take account of the location of the receiver, and to check the strength of the various diffracted components, before any of them may be neglected.

For source and receiver positions more relevant to those in an auditorium, Fig. 18 shows the field scattered by the barrier as a function of the frequency. The typical pattern of the filter comb is due to the interference of the edge diffracted waves and the wave that is double-specularly reflected at the corner made by the wall and the barrier. This effect is seen to diminish in significance at higher frequencies where, according to Fig. 17, the amplitude of the edge diffracted field reduces appreciably.

Fig. 19 illustrates the variation of the scattered field with distance for a fixed position of the sound source as the receiver moves away from the wall, on a line normal to it.

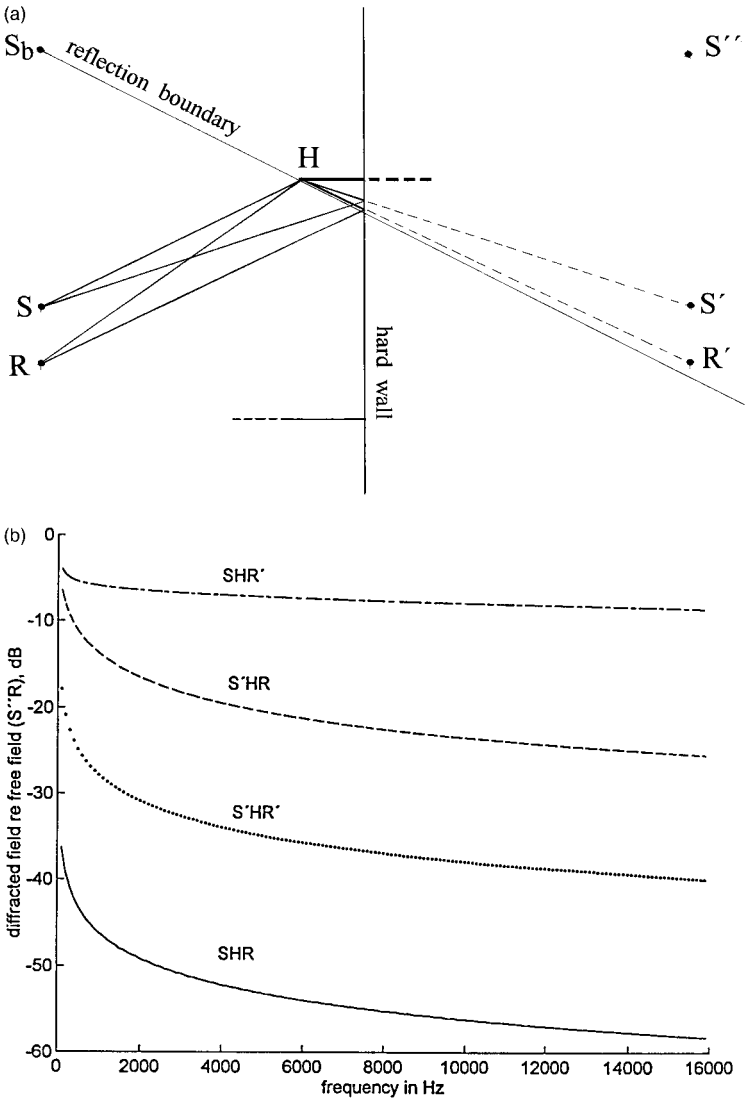

Fig. 17. (a) geometry for a horizontal thin barrier on a wall; (b) amplitude of the four different components of the diffracted field as normalised to the free field at the distance S′′R.

9. Discussion and conclusions

The pressure field from a point source and scattered by a thin hard barrier on a hard plane has been evaluated by means of three different approaches, originally developed for the diffraction by a half plane. Of these approaches, two are approximate and in the frequency domain while the third one is exact and in the time

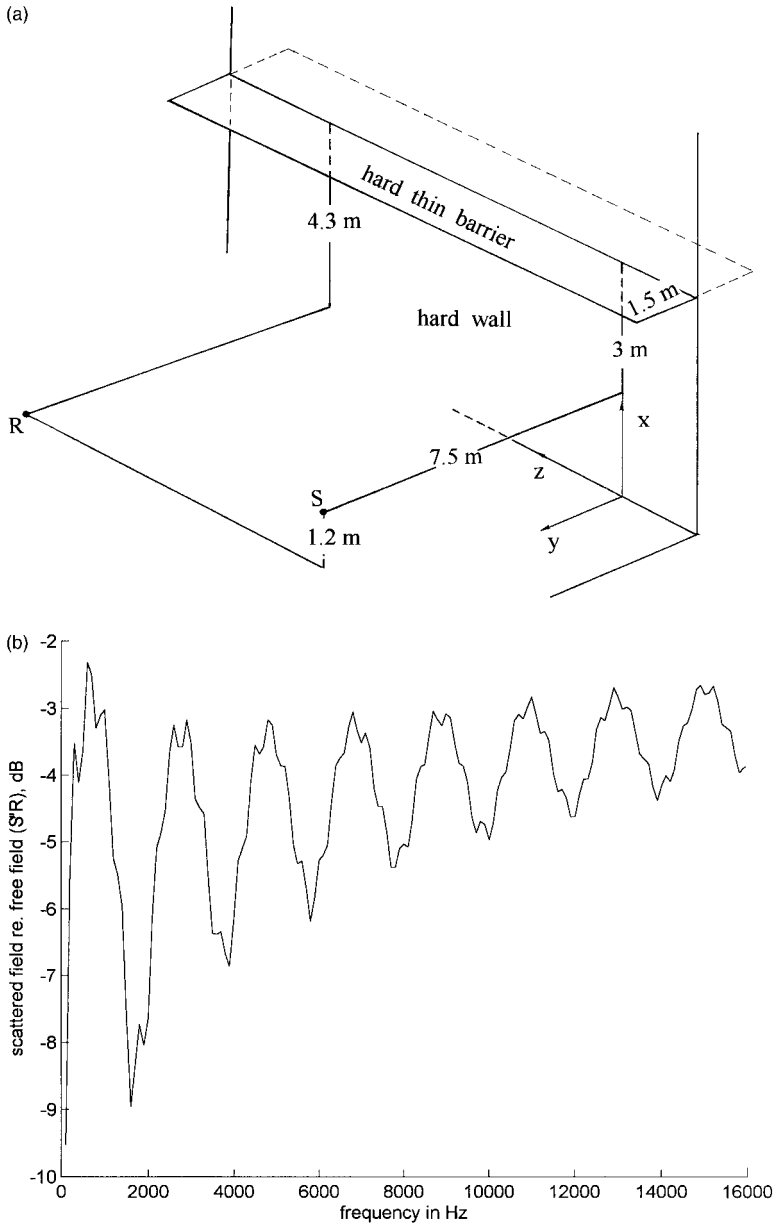

Fig. 18. Frequency dependence of the spectrum of the field scattered by a barrier on a wall.

domain. The scattered field is defined in this context as the contribution of the barrier to the total field, i.e. it is given as the difference between the fields with and without the barrier on the plane. With the help of geometrical constructions, the scattered field may be considered to result from specular reflection at the plane-barrier corner

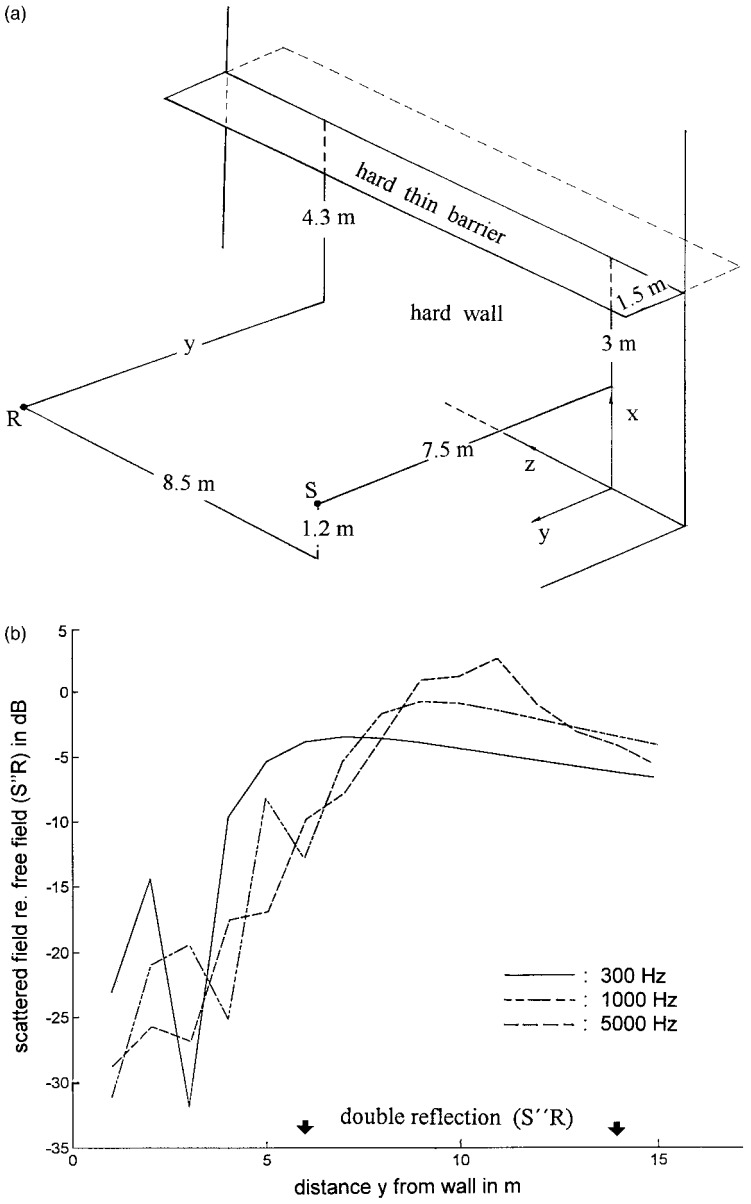

Fig. 19. Field scattered by a barrier on a wall: variation with distance from wall.

and the contribution of the fields diffracted by the edge of the barrier. To give a more qualitative and quantitative assessment of the contribution of the barrier to the pressure field, the scattered pressure has been normalised to the free field. The source-receiver distance in free field is taken as being equal to the sum of the normal distances of the source and of the receiver to the intersection of the barrier and the plane.

An improvement of high frequency results towards lower frequencies was made by taking the multiple diffraction at the edge of the barrier into consideration. As a consequence, it is expected that the theoretical predictions lose of their reliability somewhere in the low frequency range. This limit is however difficult to predict, in the absence of exact solutions. Researchers in this field resort most often to the use of numerical techniques or approximate calculation models for practical engineering purposes; for example the control of traffic noise by noise screens. The Green's function model is accurate enough and seems sufficient for the treatment of this kind of problems in the frequency domain. On the other hand, the improved approximation to the B–T theory applies almost for all frequencies and for all positions of the receiver point except at the immediate vicinity of the geometrical boundaries. Moreover, the B–T approach was originally developed for impulse excitations so has the important advantage in the prediction and the processing of impulse responses. The GTD has also been successfully used in solving electromagnetic diffraction problems, but in that case the wavelengths are several orders of magnitude smaller than their acoustical counterparts. So, to the best of our knowledge, only careful experiments can decide to what extent a given theoretical approach gives better predictions.

In those cases, where only the waves diffracted by the top of the barrier contribute to the scattered field, the spectrum of this field is seen to present some dips (e.g. Figs. 8 and 9). For various combinations of source and receiver positions (cf. Fig. 5, trajectories SHR, S′HR, S′HR and S′HR′), the impulse response exhibits four peaks of different strengths. In the frequency domain this represents a sort of comb filter effect. It is important, particularly in room acoustical applications, to know which components of the diffracted field have comparable strengths in order to avoid strong interference phenomena causing tone coloration effects. When multiple diffraction is taken into account, the response at these dips is less severe and this is well noticed at the first dips in Figs. 9 and 10. Improvements to the Green's function approach, whose single diffraction performance is already quite satisfactory, allowing for double and triple diffraction amount to about 0.5 dB at the lowest kh values and diminish as expected for higher kh values.

Two main observations may be made from the polar diagrams in Fig. 15. The first is that the scattered field exhibits a main lobe centred about the line joining the corner plane-screen and the point source with a relative level of around -3 dB. The second feature is that as the frequency increases, this main lobe becomes narrower, its peak increases and there appear other sidelobes of smaller magnitude. Hence, the idea of assimilating the scattered field as though it results from a fictive directional source at the double image source S″ seems to be reasonable.

For applications in room acoustics, the foregoing discussion elements may be summarised as follows. The scattered field of a barrier on a wall exhibits its largest contribution in the positions aligned with the source and the corner. For other positions, there is an enhancement of the low frequency components (e.g. Fig. 13). This may be used to some advantage in room acoustics. Indeed, some earlier study has shown that for a high pass band limited white noise, spaciousness (sometimes referred to also as source broadening or Raumlichkeit) increases as the lower cut-off

frequency of the noise decreases below 510 Hz [22]. This increase is especially noticeable for the frequency components around 100 to 200 Hz. In our 1/16th scale model study, 510 Hz corresponds to $kh = 15$ and 100–200 Hz to $kh \cong 3$–6 (see Figs. 8–10, 13, and 14). Spaciousness which is a highly praised effect and a subjective measure of decisive quality ranking of halls is induced by early lateral reflections [23–25] and is monitored by the arrival time and the level of these early reflections relative to that of the direct signal (see Fig. 20).

To support the claim that the scattered field contributes to the impression of spaciousness, refer to Fig. 20. The sound pressure level of the scattered field relative to that of the direct field has been calculated for practical situations. Both the time delay and the level of the scattered field relative to the direct signal have been found to lie well within the range of validity.

The point source for which the theoretical calculations were made, is difficult to realise experimentally. Considerable disagreements have been found between measured and calculated values of the scattered field. This is caused by among others the fact that at large values of the measurement angle, φ in Fig. 5, the scattered pulse could not easily be separated from the direct and the reflected pulses. Therefore, the impulse responses with and without the screen have been measured and the FFT applied to the result of their subtraction. Some traces from the direct and the reflected pulses still persisted, but were eliminated by multiplying by a suitable tapering window, leading to values of the normalised scattered field that lie within an error margin of 2 to 8 dB. The time window in question was a double sided half cosine one and this window was also used to eliminate the effect of wave diffraction at the far edges of the reflecting plane.

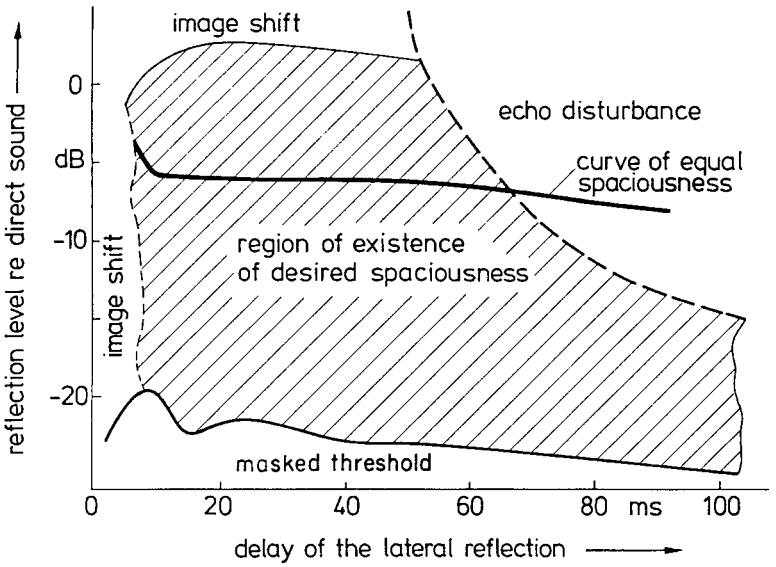

Fig. 20. Region of existence of desirable spaciousness. Direct sound plus one asymmetric echo (from [26]).

At very low frequencies, the disagreements between theoretical predictions and measurements could be attributed to several reasons. The GTD, for instance, treats the diffraction as if it were a local phenomenon. The diffracted field by a sharp edged object is the same regardless of its size with respect to the wavelength. However, this assumption is not always true for the reason that around the geometrical boundaries there exist transition zones where the GTD becomes completely unreliable and the angular breadth of these regions is proportional to the wavelength [9]. Hence, one should expect, at very low frequencies, that the receiver is situated in at least one of these very zones. Consideration of multiple diffraction is helpful but still offers limited success. On the other hand, the B–T theory is exact only for the case of the hard half plane. Its use for a finite sized barrier is not well-founded although taking into account the multiple diffraction improves the predicted value of the scattered field.

The reflecting plane used in the experiments was finite in size and not ideally hard. The poor performance of the loudspeaker at low frequencies is another source of eventual measurement errors. The apparently anomalous behaviour of the scattered field with the quite substantial disagreements with its theoretical prediction at the lowest frequencies could be due to the onset of vibrations in the structural elements used in the experiments, especially in the thin barrier (this was a band cut from a 1 mm thick aluminium plate corresponding to a surface weight of 2.7 kg/m^2). In fact, a wave impinging obliquely on an elastic panel may interact strongly with it depending on its surface mass and its radiation characteristics, to name only the most important factors.

Lastly, at an incidence angle that is not too far from the normal, it may be safely assumed that a finite hard plane is large enough for geometrical reflections to occur at it only when at least the first half Fresnel-zone can be fully contained in it [27]. One can then conclude that for a wave falling not too obliquely on the scattering barrier set on the wall, and for a source and receiver at distances not too far from it, the theoretical models developed for the diffraction by half planes may be used to predict the scattered field for wavelengths up to about half the width of the barrier.

Acknowledgements

The author wishes to express his sincere and deep gratitude to Professor Sven G. Lindblad, his Ph.D. thesis supervisor, for instigating this research project and for his continuous support until its full achievement. This work was partly financed by the Swedish Council for Building Research, BFR, and this is gratefully acknowledged.

Appendix A. Expression of the diffracted field according to the B–T theory for the case of a half plane and $z = 0$ [Eq. (6)]

This case is of the most usual occurrence in experimentation and a simplification of the complicated expression is often desired. With $\theta_W = 2\pi$, Eq. (3) becomes

$$u_d(t) = \frac{-S\rho c}{8\pi^2}\{\beta\}\frac{1}{rr_0 \sinh y}\mathrm{e}^{-y/2} \tag{A1}$$

Where β as given in Eq. (5) may be expressed again as:

$$\begin{aligned}\{\beta\} &= \frac{\sin[(\pi \pm \theta \pm \theta_0)/2]}{1 - 2\mathrm{e}^{-y/2}\cos[(\pi \pm \theta \pm \theta_0)/2] + \mathrm{e}^{-y}} \\ &= \frac{\sin[(\pi \pm \theta \pm \theta_0)/2]}{2\mathrm{e}^{-y/2}\{\cosh(y/2) - \cos[(\pi \pm \theta \pm \theta_0)/2]\}}\end{aligned} \tag{A2}$$

with (Ref. [5] f. 1.622.6, p. 47):

$$y = \operatorname{arccosh} a = \log\left[a + \sqrt{a^2 - 1}\right]; \quad a = \frac{c^2t^2 - \left(r^2 + r_0^2\right)}{2rr_0} \tag{A3}$$

$$\cosh(y/2) = \sqrt{(\cosh y + 1)/2} \tag{A4}$$

$$\sinh y = \frac{\mathrm{e}^y - \mathrm{e}^{-y}}{2} = \sqrt{\cosh^2 y - 1} = \sqrt{a^2 - 1} \tag{A5}$$

For the different sign combinations in the argument of sin and cos of $(\pi \pm \theta \pm \theta_0)/2$ one gets:

	$++$	$+-$	$-+$	$--$
$\sin[(\pi \pm \theta \pm \theta_0)/2]$	$\cos+$	$\cos-$	$\cos-$	$\cos+$
$\cos[(\pi \pm \theta \pm \theta_0)/2]$	$-\sin+$	$-\sin-$	$\sin-$	$\sin+$

with

$$\begin{matrix}\cos \\ \sin\end{matrix} \pm = \begin{matrix}\cos \\ \sin\end{matrix}\left(\frac{\theta}{2} \pm \frac{\theta_0}{2}\right)$$

Hence,

$$\{\beta\} \sim \frac{1}{2}\left[\frac{\cos+}{x + \sin+} + \frac{\cos-}{x + \sin-} + \frac{\cos-}{x - \sin-} + \frac{\cos+}{x - \sin-}\right] \tag{A6}$$

where $x = \cosh(y/2) = \sqrt{(a+1)/2}$. β then becomes:

$$\{\beta\} \sim x\left[\frac{\cos+}{x^2-\sin+^2}+\frac{\cos-}{x^2-\sin-^2}\right] \tag{A7}$$

and $u_d(t)$ takes then the form:

$$u_d(t) = \frac{-S\rho c}{8\pi^2}x\left[\frac{\cos+}{x^2-\sin+^2}+\frac{\cos-}{x^2-\sin-^2}\right]\frac{1}{rr_0\sqrt{a^2-1}} \tag{A8}$$

Next:

$$rr_0\sqrt{a^2-1} = rr_0\left\{\left[\frac{c^2t^2-\left(r^2+r_0^2\right)}{2rr_0}\right]^2-1\right\}^{1/2} = \frac{c^2}{2}\sqrt{\left(t^2-t_+^2\right)\left(t^2-t_-^2\right)} \tag{A9}$$

with:

$$t_\pm = (r \pm r_0)/c \tag{A10}$$

and because:

$$rr_0 = \frac{c^2\left(t_+^2-t_-^2\right)}{4} \tag{A11}$$

x may then be expressed this time in terms of t_+ and t_-, namely:

$$x = \cosh(y/2) = \sqrt{(a+1)/2} = \frac{c}{2}\sqrt{\left(t^2-t_-^2\right)/rr_0} = \sqrt{\left(t^2-t_-^2\right)\left(t_+^2-t_-^2\right)} \tag{A12}$$

Then, inserting (A9) and (A11) in (A8) leads to:

$$\begin{aligned} u_d(t) = \frac{-S\rho}{4\pi^2 c}\sqrt{\frac{t_+^2-t_-^2}{t^2-t_+^2}}\Bigg\{ & \frac{\cos[(\theta+\theta_0)/2]}{t^2-t_-^2-\left(t_+^2-t_-^2\right)\sin^2[(\theta+\theta_0)/2]} \\ & +\frac{\cos[(\theta-\theta_0)/2]}{t^2-t_-^2-\left(t_+^2-t_-^2\right)\sin^2[(\theta-\theta_0)/2]} \end{aligned} \tag{A13}$$

which when using $\sin^2 = 1-\cos^2$ gives Eq. (6).

The expression for the short time range after the least time $\tau_0 = t_+ = (r+r_0)/c$, is given as an expressin of $\tau = t - t_0$ with the following considerations:

$$\begin{aligned} &\tau = t - \tau_0 = t - t_+ \;\Rightarrow\; t = \tau + t_+ \\ &t^2 - t_+^2 = (t - t_+)(t + t_+) = \tau(\tau + 2t_+) \;\underset{\tau \to 0}{\to} 2\tau t_+ \end{aligned} \tag{A14}$$

$$\begin{aligned} t^2 - t_-^2 &= (t - t_-)(t + t_-) = (t - t_+ + t_+ - t_-)(t - t_+ + t_+ + t_-) \\ &= [\tau + (t_+ - t)](\tau + t_+ + t_-) \underset{\tau \to 0}{\to} \left(t_+^2 - t_-^2\right) \end{aligned} \tag{A15}$$

and the approximation for (A13) becomes then:

$$u_d(\tau) \approx \frac{-S\rho}{4\pi^2 c} \frac{1}{\sqrt{2t_+\left(t_+^2 - t_-^2\right)}} \left\{ \frac{1}{\cos[(\theta + \theta_0)/2]} + \frac{1}{\cos[(\theta - \theta_0)/2]} \right\} \cdot \frac{1}{\sqrt{\tau}} \tag{A16}$$

which is the expression of Eq. (8).

Appendix B. Expression of erfc $\left(\sqrt{-i\omega a}\right)$ in terms of the Fresnel integrals for a real positive argument

For the complex argument $z = \left(\sqrt{-i\omega a}\right) = (1-i)\sqrt{\pi f a}$ ($f = \omega/2\pi$ is the frequency) the function defined by:

$$\operatorname{erfc}(z) = \frac{2}{\sqrt{\pi}} \int_z^\infty \mathrm{e}^{-u^2} \mathrm{d}u \tag{B1}$$

is sometimes not available in calculation software and reformulation using available functions is desirable. Starting from the following expressions (Ref. [28] f. 7.1.3 p. 299, and f. 7.3.22 p. 301):

$$\operatorname{erfc}(-iz) = \mathrm{e}^{z^2} w(z) \tag{B2}$$

$$C(x) + iS(x) = \frac{1+i}{2} \left\{ 1 - e^{i\pi x^2/2w} \left[\frac{\sqrt{\pi}}{2} (1+i)x \right] \right\} \tag{B3}$$

where the Fresnel cosine and sine integrals are defined by:

$$\mathrm{C, S}(x) = \int_0^x \cos, \sin\left(\frac{\pi}{2} u^2\right) \mathrm{d}u \tag{B4}$$

and after setting $z = (1+i)\sqrt{\pi f a}$ in (B1), and rearranging (B3) one gets finally:

$$\operatorname{erfc}\left(\sqrt{-i\omega a}\right) = \operatorname{erfc}\left[\sqrt{-i2\pi fa}\right] = 1 - \frac{2}{1+i}[\mathrm{C}(x) + i\mathrm{S}(x)] \tag{B5}$$

or:

$$\operatorname{erfc}\left(\sqrt{-i\omega a}\right) = \operatorname{erfc}\left[\sqrt{-i2\pi fa}\right] = 1 - [\mathrm{C}(x) + \mathrm{S}(x)] + i[\mathrm{C}(x) - \mathrm{S}(x)] \tag{B6}$$

with $x = 2\sqrt{fa}$.

Appendix C. Development of $A_D(P) = f(P) - ig(P)$ in Eq. (39)

$$A_D(P) = \frac{P}{\sqrt{\pi}} \int_0^{\infty} \frac{\mathrm{e}^{-u^2}}{\frac{\pi}{2}P^2 + iu^2}\,\mathrm{d}u \tag{C1}$$

$$A_D(P) = \frac{iP}{\sqrt{\pi}} \int_0^{\infty} \frac{\mathrm{e}^{-u^2}}{z^2 - u^2}\,\mathrm{d}u = \frac{iP}{\sqrt{\pi}} \cdot \frac{\pi}{2iz} w(z) \tag{C2}$$

with:

$$z = \frac{\sqrt{\pi}}{2}(1+i)|P| \tag{C3}$$

and $w(z)$ defined by [28]:

$$w(z) = \frac{i}{\pi} \int_{-\infty}^{+\infty} \frac{\mathrm{e}^{-u^2}}{z-u}\,\mathrm{d}u = \frac{2iz}{\pi} \int_0^{\infty} \frac{\mathrm{e}^{-u^2}}{z^2 - u^2}\,\mathrm{d}u \tag{C4}$$

(C2) becomes then:

$$A_D(P) = \frac{iP}{\sqrt{\pi}} \frac{\pi}{2i\frac{\sqrt{\pi}}{2}(1+i)|P|} w(z) = \frac{\operatorname{sgn}(P)}{(1+i)} w\left[\frac{\sqrt{\pi}}{2}(1+i)|P|\right] \tag{C5}$$

Hence, using (B3), (C5) reads then as:

$$A_D(P) = \operatorname{sgn}(P) e^{i\pi P^2/2} \left\{\frac{1}{2} - S(|P|) - i\left[\frac{1}{2} - C(|P|)\right]\right\} = f(P) - ig(P) \tag{C6}$$

with:

$$f, g(P) = \mathrm{sgn}(P) e^{i\pi P^2/2} \left[\frac{1}{2} - S, C(|P|) \right] \tag{C7}$$

Appendix D. The double diffraction for the B–T theory applied to the hard thin strip on the reflecting plane

With reference to Fig. D1, the pulse emitted by the source S travels along the least path via the edge of the wedge towards R contributing there to a large amount of the diffracted energy. Later arrival of the remaining energy comes from points situated on the edge on both sides of the least time point and this is due to the delayed arrival of the front of the initial pulse to these points. Hence, the idea would be to discretise these contributions by considering the edge as containing an infinite set of secondary sources, SSs, having different strengths and emitting at discrete lapses of time [29].

If one chooses the time interval as ΔT, then one defines new source-edge-receiver paths lagging behind the least time path by discrete values $n\Delta T$ and the contribution of the nth SS to the received pressure is defined as the mean of $u_d(\tau)$ centred at $n\Delta T$ and of duration ΔT i.e.:

$$< u_d(n\Delta T) >= \frac{1}{\Delta T} \int_{(n-\,1/2)\Delta T}^{(n+\,1/2)\Delta T} u_d(\tau) \mathrm{d}\tau \tag{D1}$$

If the field point is not near the shadow boundary, that is near the plane containing the edge of the wedge and the point source (in which case the discrete diffracted pulse becomes a delta function), then for $n=0$, and taking the lower limit in the integral to be zero, Eq. (D1) becomes:

$$< u_d(\tau_0) > \sim 1/(\Delta T)^{1/2} \tag{D2}$$

For $n \geqslant 1$, one can safely take the instantaneous values $u_d(n\Delta T)$ instead of the average values; the committed error being max 3.5% (for $n = 1$) as long as one is far from the geometrical shadow boundaries (usually a few degrees suffice) [29]. For every $n \geqslant 1$, the SSs occur in pairs, the strengths of which being:

$$S_{SSn} = F_n S \tag{D3}$$

where S is the strength of the original source entering in Eq. (1) and:

$$F_n = \frac{1}{2} < u_d(n\Delta T) > / u_\delta \tag{D4}$$

with:

$$\begin{aligned} u_\delta &= S\rho/(2\pi R\Delta T) \quad \text{Receiver on plane of wedge} \\ u_\delta &= S\rho/(4\pi R\Delta T) \quad \text{Receiver not on plane wedge} \end{aligned} \tag{D5}$$

and where R is the distance from the secondary source to the receiver. For the more general case and with reference to Fig. D1, the secondary source fractions F_n and $F_{n'}$ are given by the following expressions:

$$F_n = \frac{< u_d(n\Delta T) >}{u_\delta} \cdot \frac{r_{0n} r_n}{r_{0n} r_n + r'_{0n} r'_n}; \; F'_n = \frac{< u_d(n\Delta T) >}{u_\delta} \cdot \frac{r'_{0n} r'_n}{r_{0n} r_n + r'_{0n} r'_n} \tag{D6}$$

The application of these preliminary results to the double diffraction by the barrier on the plane is illustracted in Fig. D2 where $\mathrm{H_n}(0, h, z_n)$ is the position of the n_{th} SS and $\mathrm{H_{in}}(0, -h, z_n)$ its image through the plane. After reflection on the plane, the pulse of the n_{th} SS returns to the edge where a second order diffracted wave emanates. Thus one can consider as if the n_{th} SS's pulse originates at $\mathrm{H_{in}}$.

In its original presentation [29], the $\mathrm{H_n}$s are defined in a way such that:

$$\mathrm{SH_n} + \text{least path of } (\mathrm{H_{in}} - \text{edge} - \mathrm{R}) - \mathrm{SHR} = c \cdot n \cdot \Delta T$$

or using the geometry of Fig. D2:

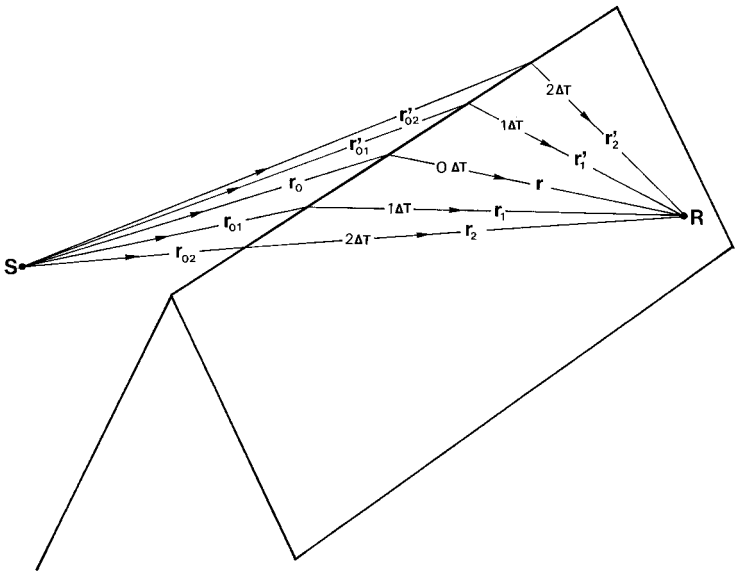

Fig. D1. Interpretation of the diffraction by a wedge as the contribution of discrete secondary sources on the wedge.

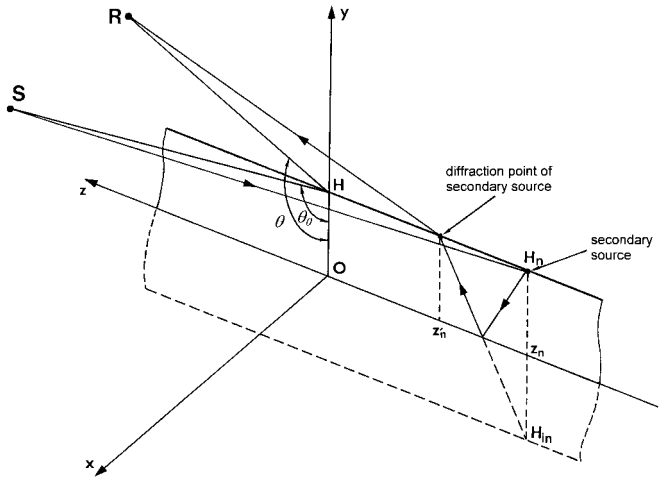

Fig. D2. Geometry of the double diffraction for a barrier on a plane.

$$\sqrt{r_0^2 + z_n^2} + \left[(2h + r)^2 + z_n^2\right]^{1/2} - (r + r_0) = c \cdot n \cdot \Delta T \tag{D7}$$

the solution of which is given by:

$$z_n = \left\{ \left\{ \left(R'^2/2\right)^2 - \left[r_0(2h + r)\right]^2 \right\} / \left[r_0^2 + (2h + r)^2 + R'^2\right] \right\}^{1/2} \tag{D8}$$

with:

$$R'^2 = \left[cn\Delta T + (r + r_0)\right]^2 - r_0^2 - (2h + r)^2 \tag{D9}$$

and subject to the constraints:

$$z_n^2 \leqslant (cn\Delta T)^2/2 - cn\Delta T(r + r_0) + rr_0 - 2h(h + r) \tag{D10}$$

$$\left[cn\Delta T + (r + r_0)\right]^2 \geqslant r_0^2 + (2h + r)^2 \tag{D11}$$

The solution to Eq. (D7) may also be obtained numerically. From Fig. D2, making the distance H_{in}–edge–R shortest leads to an equation of the second order in z'_n

$$z_n'^2(4h^2 - r^2) + 2z_n z'_n r^2 - z_n^2 r^2 = 0 \tag{D12}$$

For which the solution leads to a simple relation between z'_n and z_n given by:

$$z'_n = z_n \frac{r}{r+2h} \tag{D13}$$

The strengths of the SS′s are calculated through using Eq. (A16) for $n = 0$ and Eq. (A13) for $n \geqslant 1$. Important temporal quantities to be considered are first the time of emission of the diverse SSs.

$$T_{0n} = \sqrt{r_0^2 + z_0^2}/c \tag{D14}$$

after the arrival of the original pulse's wavefront from S, and the time of arrival of the doubly diffracted pulse:

$$T_{0n} + \tau_{0n}$$

with:

$$\tau_{0n} = \sqrt{(r+2h)^2 + z_n^2}/c \tag{D15}$$

which means that considering for a first approximation that the SSs are not too far from the y axis (through choosing small values of ΔT and n), t and τ in (A16) and (A13) are to be respectively replaced by:

$$t_n = t - T_{0n} \tag{D16}$$

and:

$$\tau_n = t_n - \tau_{0n} \tag{D17}$$

The pressure radiated by the n_{th} SS in this case may be than expressed as:

$$u_{SSn} = \frac{\rho S_{SSn}}{4\pi R_n} \delta(t_n - R_n/c) \tag{D18}$$

with R_n, the distance range to the field point, being given by:

$$R_n = \sqrt{r^2 + z_n^2} \tag{D19}$$

and:

$$S_{SSn} = F_n S = \frac{1}{2} \frac{< u_d(n\Delta t) >}{u_\delta} S = \frac{< u_d(n\Delta T) > \pi R_n \Delta T}{\rho} \tag{D20}$$

For $n=0$ the 1/2 in (D20) is omitted and using Eq. (A16), after some mathematical operations gives:

$$U_{SS0}=\frac{\rho S_{SS0}}{4\pi c}\delta(t_0-R_0/c);\ S_{SS0}=\frac{-SR_0}{\pi c}\sqrt{\frac{\Delta T}{t_+\cdot\left(t_+^2-t_-^2\right)}}\left\{\frac{1}{\cos_\pm}\right\}_+ \tag{D21}$$

i.e.:

$$u_{SS0}=\frac{\rho S}{4\pi R_0}\frac{R_0}{R_0'}\delta(t_0-R_0/c) \tag{D22}$$

where R_0' is a distance parameter given by:

$$R_0^{'-1}=-\frac{1}{\pi c}\sqrt{\frac{\Delta T}{t_+\cdot\left(t_+^2-t_-^2\right)}}\left\{\frac{1}{\cos\pm}\right\}_+ \tag{D23}$$

and for simplicity, as before, the book, the hook $\{\}_+$ represents the sum of two terms. Then, applying the primary results of the diffracted field to this new source, that is writing (A13) and (A16) for the new source described by Eq. (D22).

$$u_{d0}(t_0)=2\frac{-S\rho}{4\pi^2 c}\frac{2h}{R_0'}\sqrt{\frac{t_{+0}^2-t_{-0}^2}{t_0^2-t_{+0}^2}}\cdot 2\frac{\cos(\theta/2)}{t_0^2-t_{-0}^2-\left(t_{+0}^2-t_0^2\right)\sin^2(\theta/2)} \tag{D24}$$

and:

$$u_{di0}(\tau_0)=2\frac{-S\rho}{4\pi^2 c}\frac{2h}{R_0'}\frac{1}{\sqrt{2t_{+0}\cdot\left(t_{+0}^2-t_{-0}^2\right)}}\cdot 2\cdot\frac{1}{\cos(\theta/2)}\cdot\frac{1}{\sqrt{\tau_0}} \tag{D25}$$

because $r_0=2h$ and $\theta_0=0$, and the multiplicative factor 2 is owing to the parity of the SSs.

For $n\geqslant 1$, one cannot in general use Eq. (A16) because one does not have in advance an idea on how much the approximate short time expression departs from the exact one. Reformulating the exact expression of the diffracted field in Eq. (A13) as:

$$u_d(t)=\frac{-S\rho}{4\pi^2 c}2c\cdot\sqrt{\frac{rr_0}{t^2-\tau_0^2}}\left\{\frac{\cos\pm}{4rr_0\cos^2\pm+c^2\left(t^2-\tau_0^2\right)}\right\}_+ \tag{D26}$$

and of its approximation in Eq. (A16):

$$u_{di}(\tau)=\frac{-S\rho}{4\pi^2 c}c\cdot\sqrt{\frac{rr_0}{2\tau_0\tau}}\left\{\frac{\cos\pm}{2rr_0\cos^2\pm+c^2\tau_0\tau}\right\}_+ \tag{D27}$$

then, one uses for the S_{SSn} the expression of the instantaneous pressure rather than its mean in the form given in Eq. (D20). Hence, setting t equal to $\tau_0 + n\Delta T$ in Eq. (D26) gives:

$$< u_d(n\Delta T) > = \frac{-S\rho}{4\pi^2 c}\frac{2c}{n\Delta T}\sqrt{\frac{rr_0}{1+2\tau_0/n\Delta T}} \cdot\left\{\frac{\cos\pm}{4rr_0\cos^2\pm + (cn\Delta T)^2(1+2\tau_0/n\Delta T)}\right\}_+ \tag{D28}$$

From this last expression, it is well noticed that $< u(n\Delta T) >$ becomes smaller the larger is n. Inserting Eq. (D28) in Eq. (D18), the pulse radiated by the n_{th} SS may then be expressed as:

$$u_{SSn} = \frac{\rho S}{4\pi R_n}\cdot\frac{R_n}{R'_n}\delta(t_n - R_n/c) \tag{D29}$$

where:

$$R_n^{'-1} = -\frac{1}{\pi n}\sqrt{\frac{rr_0}{1+2\tau_0/n\Delta T}}\left\{\frac{\cos\pi}{4rr_0\cos^2_{\pm} + (cn\Delta T)^2(1+2\tau_0/n\Delta T)}\right\}_+ \tag{D30}$$

Then, using Eqs. (D26) and (D27) for this expression of the unit pulse one gets:

$$u_{dn}(t_n) = 2\frac{-S\rho}{4\pi^2 c}\frac{R_n}{R'_n}2c\sqrt{\frac{r2h}{t_n^2 - \tau_{0n}^2}}\cdot 2\cdot\frac{\cos(\theta/2)}{4r2h\cos^2(\theta/2) + c^2\left(t_n^2 - \tau_{0n}^2\right)} \tag{D31}$$

and:

$$u_{din}(\tau_n) = 2\frac{-S\rho}{4\pi^2 c}\frac{R_n}{R'_n}c\sqrt{\frac{r2h}{2\tau_{0n}}}\cdot 2\cdot\frac{\cos(\theta/2)}{2r2h\cos^2(\theta/2) + c^2\tau_{0n}\tau_n}\cdot\frac{1}{\sqrt{\tau_n}} \tag{D32}$$

The factor 2 in front of the expression comes as before from the parity occurrence of the SSs.

In the case of the new short range time approximation of the diffracted field, one uses Eq. (15) instead of Eq. (A16) to evaluate the partial strength of the SSs.

For $n = 0$, the form corresponding to (D22) is:

$$S_{SS0} = -\frac{SR_0}{\pi c}\sqrt{\frac{t_+^2 - t_-^2}{2t_+}}\frac{1}{t_+}\left\{\frac{\cos\pm}{\sqrt{a_\pm}}\arctan\sqrt{\frac{\Delta T/2}{a_\pm} - \frac{\pi}{4}}\right\}_+ \tag{D33}$$

whereas for $n \geqslant 1$, the relative SS's strength becomes:

$$S_{SSn} = -\frac{SRn}{2\pi c}\sqrt{\frac{t_+^2 - t_-^2}{2t_+}}\frac{1}{t_+} \left\{\frac{\cos_\pm}{\sqrt{a_\pm}}\left(\arctan\sqrt{\frac{(n+1/2)\Delta T}{a\pm}} - \arctan\sqrt{\frac{(n+1/2)\Delta T}{a\pm}}\right)\right\}_+ \tag{D34}$$

with $a^\pm = \frac{t_+^2 - t^2}{2t_+}\cdot\cos_\pm^2$. These last two expressions result from an integration of the form:

$$\int \frac{1}{\sqrt{\tau}}\cdot\frac{1}{\tau + a}\,\mathrm{d}\tau = \frac{2}{\sqrt{a}}\arctan\sqrt{\frac{\tau}{a}};\quad a > 0 \tag{D35}$$

The numerical treatment of our problem by the double diffraction approach is handled in the optimal way. The SS′s strengths are calculated by means of the new $u_{di}(\tau)$ [Eqs. (D33) and (D34)] because of the more realistic conditions than those taking the values of the pressure rather than its mean at $n\Delta T$ in (D28), and giving more reliable values than when using the primary form of u_{di} in (A16) or (D27). Then for the o_{th} SS, Eqs. (A13) and (A16) are, respectively, used for the exact and for the initial doubly diffracted pressure. For the n_{th} SS ($n \geqslant 1$) these correspond respectively to (D26) and (D25).

The calculations done at this stage consider the case of one pair of a point source and a field point. In the problem we are treating, we have to extend these results to the three other combinations of the real points and their images. In the following theses are taken into account by adding an integer $1 \leqslant m \leqslant 4$ as a superscript in the field quantities in (D24), (D25), and (D32), and the corresponding quantities resulting from using (D33) and (D34) should not be forgotten due to the possibility of the diffracted fields to propagate also behind the thin screen.

All what is left now is to translate these results in the frequency domain. The single diffracted fields are expressed in forms given by Eqs. (A13) and (A16). Then the total diffracted field $u_{d\mathrm{tot}}$ is given by:

$$u_{d\mathrm{tot}}(t) = \sum_{m=1}^{4}\left\{u_d^m(t)H(t - t_+^m) + \sum_{n=0}^{n} u_{dn}^m(t_n^m)H\left[t^m - (T_{n0}^m + \tau_{0n}^m)\right]\right. \tag{D36}$$

where $H(t)$ is the unit step Heaviside function:

$$H(t) = \begin{cases} 0 & t \leqslant 0 \\ 1 & t > 0 \end{cases} \tag{D37}$$

The Fourier transform (FT) of (D36) reads then as:

$$u_{d\mathrm{tot}}(f) = FT[u_{d\mathrm{tot}}(t)] = \int_{-\infty}^{+\infty} u_{d\mathrm{tot}}(t)\mathrm{e}^{i\omega t}\mathrm{d}t \tag{D38}$$

and by using the same arguments as those which led to Eq. (13) we divide the total FT into an analytical part of the initial diffracted pressures $u_{di}^{m}(\tau)$ and $u_{din}^{m}(\tau_n)$ and a digital FT of the left part $\Delta u_{d\mathrm{tot}}(t)$ with a suitable smoothing window. Practically, a length of one or two seconds is sufficient to include most of the information to the FFT analysis. This is so because for the geometry of the study examples, the diverse τ_0 are in the order of the millisecond and the maxima in the $\Delta u_d(t)$ occur near τ_0, so at a time of 1 s after τ_0 the requirement $\Delta u_d\,(1\text{ s}) = 5\%\ \Delta u_d(t)_{\max}$ is largely satisfied. Moreover, in practice a maximal frequency of some kiloHertz is sufficient. One can then choose safely a time interval sampling of 50 μs (or a sampling frequency of 20 KHz).

The time window $w(t)$ is shown in Fig. D3 and the expression of which is:

$$w(t) = \begin{cases} 1 & 0 \leqslant t < T \\ \dfrac{1}{2}\left[1 + \cos\dfrac{\pi(t-T)}{T/10}\right] & T \leqslant t \leqslant 11T/10 \\ 0 & t > 11T/10 \end{cases} \tag{D39}$$

Before giving the final FT one should represent the analytical FT of Eq. (D32), a form similar to that met earlier in (D16) and which can be expressed (with a constant factor omitted) as:

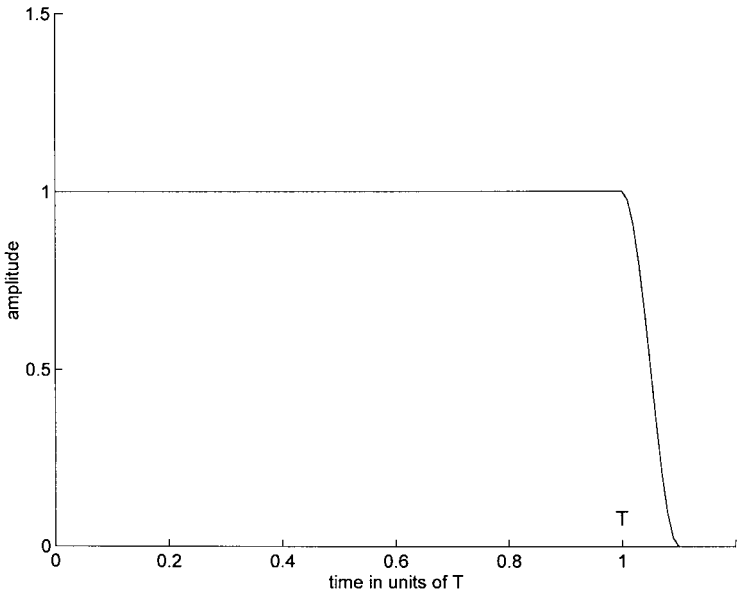

Fig. D3. The half cosine taper window.

$$\int_{-\infty}^{+\infty} \frac{1}{\sqrt{\tau_n(a+\tau_n)}} H(t_n - \tau_{0n}) e^{i\omega t_n} dt_n = \int_{\tau_{0n}}^{\infty} \frac{1}{\sqrt{\tau_n}(a+\tau_n)} e^{i\omega t_n} dt_n \tag{D40}$$

and with $\tau_n = t_n - \tau_{0n} \Rightarrow t_n = \tau_n + \tau_{on}$; $dt_n = d\tau_n$

$$FT[u_{din}(\tau_n)] \sim e^{i\omega_{0n}} \int_0^{\infty} \frac{1}{\sqrt{\tau_n}(a+\tau_n)} e^{i\omega\tau_n} d\tau_n = e^{i\omega\tau_{0n}} \frac{\pi}{\sqrt{a}} e^{-i\omega a} \operatorname{erfc}(\sqrt{-i\omega a}) \tag{D41}$$

where $\operatorname{erfc}(x)$ is the error complementary function which was seen in Appendix B for the complex argument $\sqrt{-i\omega a} = (1-i)\sqrt{\pi f a}$.

Appendix E. Multiple diffraction by the barrier on the plane using the GTD approach

In this appendix, use is made of $e^{+j\omega t}$ for the time dependence to following the same guidelines of the UTD in the original text [13]. This will not affect the final results if they are presented relative to some reference. Consider Fig. E1.

If we call $u_d^0(\varphi, r)$ the diffracted field of order zero at R due to the source S, then $u_d^0(\varphi, s)$ is expressed as:

$$u_d^0(\varphi, r) = \frac{e^{-ikr'}}{r'} D_h(\varphi', r', \varphi, r) A_{sph} e^{-ikr} \tag{E1}$$

with:

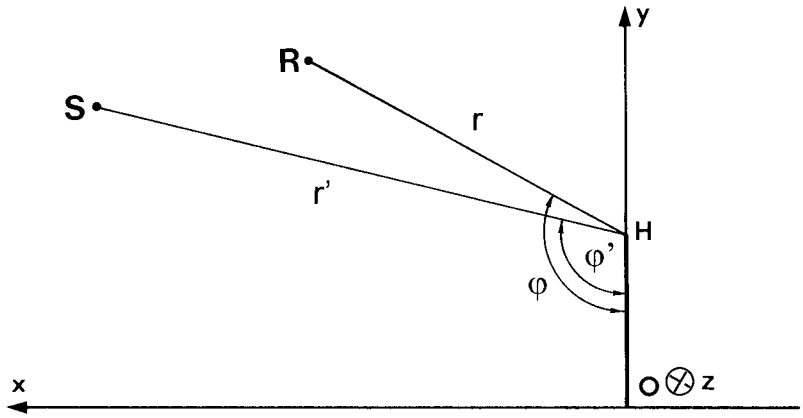

Fig. E1. Showing the parameters for the multiple diffraction.

$$D_h(\varphi', r', \varphi, r) = -\mathrm{e}^{i\pi/4}\sqrt{\frac{L(r', r)}{\pi}} \cdot \Big\{ f[kL(r', r), \varphi' - \varphi]\mathrm{e}^{2ikL(r', r)\cos^2\left[(\varphi' - \varphi)/2\right]}\mathrm{sgn}(\pi + \varphi - \varphi') + f[kL(r', r), (\varphi + \varphi')]\mathrm{e}^{2ikL(r', r)\cos^2[(\varphi + \varphi')/2]}\mathrm{sgn}(\pi - \varphi' - \varphi)\Big\} \tag{E2}$$

and:

$$A_{sph} = \sqrt{\frac{r'}{r(r + r')}} \tag{E3}$$

f is the function as defined in Eq. (26) and is considered in some more detail later.

This diffracted field gives rise to a diffracted field of first order u_d^1, the first element of the series of the multiple field, due to the propagation of the ray u_d^0 along both sides of the strip and its return back to the top H of the strip. Thus, by considering the origin of this field at the image of H through the plane, and by supposing it having a conical character, u_d^1 can be expressed as:

$$u_d^1(\varphi, r) = u_d^0(0, 2h)D_h(0, 2h, \varphi, r)A_{\mathrm{con}}\mathrm{e}^{-ikr} + u_d^0(2\pi, 2h)D_h(0, 2h, 2\pi - \varphi, r)A_{\mathrm{con}}\mathrm{e}^{-ikr} \tag{E4}$$

where:

$$A_{\mathrm{con}} = \frac{1}{\sqrt{r}} \tag{E5}$$

In Eq. (E4), the second term has taken this form because the incident ray should have an angle if incidence less than or equal to π and if one looks at Fig. E1 from the other side of the page, i.e. towards the opposite direction of the z axis, then the incidence angle becomes 0 and R is at the angle $(2\pi - \varphi)$.

By using the definition Eq. (E2) one finds that:

$$D_h(0, 2h, \varphi, r) = -D_h(0, 2h, 2\pi - \varphi, r) = = -2\mathrm{e}^{i\pi/4}\sqrt{L(2h, r)/\pi}f[kL(2h, r), \varphi]\mathrm{e}^{i2kL(2h,r)\cos^2(\varphi/2)}\mathrm{sgn}(\pi - \varphi) \tag{E6}$$

with $f(\alpha, \gamma)$ defined by:

$$f(\alpha, \gamma) = \int_x^\infty \mathrm{e}^{-i\tau^2}\mathrm{d}\tau \quad x = \sqrt{2\alpha}\left|\cos(\gamma/2)\right| \tag{E7}$$

and developed as:

$$f(\alpha,\gamma)=\int_0^{\infty}-\int_0^{x}\left[\cos(\tau^2)-i\sin(\tau^2)\right]\mathrm{d}\tau$$
$$=\sqrt{\pi/2}\left\{\left[\frac{1}{2}-C(\sqrt{2/\pi}\cdot x)\right]-i\left[\frac{1}{2}-S(\sqrt{2/\pi}\cdot x)\right]\right\} \tag{E8}$$

where again C and S are, respectively, the cosine and since Fresnel integrals defined in (B4). Hence, Eq. (E4) takes the new form:

$$u_d^1(\varphi,r)=2u_d^0(0,2h)D_h(0,2h,\varphi,r)\frac{\mathrm{e}^{-ikr}}{\sqrt{r}} \tag{E9}$$

because:

$$u_d^0(2\pi,2h)=-u_d^0(0,2h) \tag{E10}$$

which can be proved through developing Eqs. (E1) and Eqs. (E2) after setting respectively, 2π and 0 for φ in Eq. (E2). Actually, this is an important symmetry property of the diffracted field stating that at two points on the opposite sides of the diffracting half plane, the diffracted field has equal amplitudes but the phases are opposite. This can also be verified in the exact time domain expression as given by Eq. (6) in the text.

The diffracted field of the second order is derived in a similar way, namely:

$$u_d^2(\varphi,r)=u_d^1(0,2h)D_h(0,2h,\varphi,r)\frac{\mathrm{e}^{-ikr}}{\sqrt{r}}$$
$$+u_d^1(2\pi,2h)D_h(0,2h,2\pi-\varphi,r)\frac{\mathrm{e}^{-ikr}}{\sqrt{r}} \tag{E11}$$

with:

$$u_d^1(0,2h)=-u_d^1(2\pi,2h)=2u_d^0D_h(0,2h,0,2h)\frac{\mathrm{e}^{-ik2h}}{\sqrt{2h}} \tag{E12}$$

$u_d^2(\varphi,r)$ is expressed again as:

$$u_d^2(\varphi,r)=2u_d^1(0,2h)D_h(0,2h,\varphi,r)\frac{\mathrm{e}^{-ikr}}{\sqrt{r}}$$
$$=2\cdot 2u_d^0(0,2h)D_h(0,2h,0,2h)\frac{\mathrm{e}^{-ik2h}}{\sqrt{2h}}D_h(0,2h,\varphi,r)\frac{\mathrm{e}^{-ikr}}{\sqrt{r}}$$
$$=u_d^1(\varphi,r)D_h(0,2h,0,2h)\sqrt{2/h}\,\mathrm{e}^{-ikh}=u_d^1(\varphi,r)\cdot x \tag{E13}$$

$$x=D_h(0,2h,0,2h)\sqrt{2/h}\cdot\mathrm{e}^{-ik2h}$$

And by the same process one can show by induction that the diffracted field of order $n+1$ may be expressed in terms of the first order one in:

$$u_d^{n+1}(\varphi, r) = u_d^n(\varphi, r)x = u_d^1(\varphi, r)x^{n+1}, n \geqslant 1 \tag{E14}$$

The sun of all these multiply diffracted fields yields:

$$u'_d = u_d^1\left[1 + x + x^2 + \ldots.. + x^n + ..\right] \tag{E15}$$

a series which could converge only if $|x| \leqslant 1$.

By using Eq. (E6) one can show that:

$$D_h(0, 2h, 0, 2h) = -2\mathrm{e}^{i\pi/4}\sqrt{h/\pi}f(kh, 0)\mathrm{e}^{i2kh} \tag{E16}$$

and consequently the term x of the geometrical series is written again as:

$$x = D_h(0, 2h, 0, 2h)\cdot\sqrt{2/h}\,\mathrm{e}^{-ik2h} = -2\sqrt{2/\pi e^{i\pi/4}}f(kh, 0) \tag{E17}$$

with the expression of f given in Eq. (E8), x takes the form:

$$x = -\mathrm{e}^{i\pi/4}\left\{\left[1 - 2C\left(2\sqrt{kh/\pi}\right)\right] - i\left[1 - 2S\left(2\sqrt{kh/\pi}\right)\right]\right\} \tag{E18}$$

and finally the inequality.

$$|x| = \left\{\left[1 - 2C\left(2\sqrt{kh/\pi}\right)\right]^2 + \left[1 - 2S\left(2\sqrt{kh/\pi}\right)\right]^2\right\}^{1/2} \leqslant 1 \tag{E19}$$

is largely satisfied when the argument of the Fresnel functions C and S exceeds 3.5, i.e.:

$$2\sqrt{kh/\pi} \geqslant 3.5 \text{ or } kh \geqslant 10 \tag{E20}$$

Appendix F. The inclusion of double and triple diffraction in the Green's function model

This appendix is a completion of Section 5.2 where it was considered only the case of sharp edges. However, one should not exclude the possibility of noise shielding by thick barriers or many sided pillars. A simple example is drawn in Fig. F1.

Basically, the multiple diffraction is considered in the same way as with the GTD or the B–T theory, that it is an extension of the single diffraction ocurring when

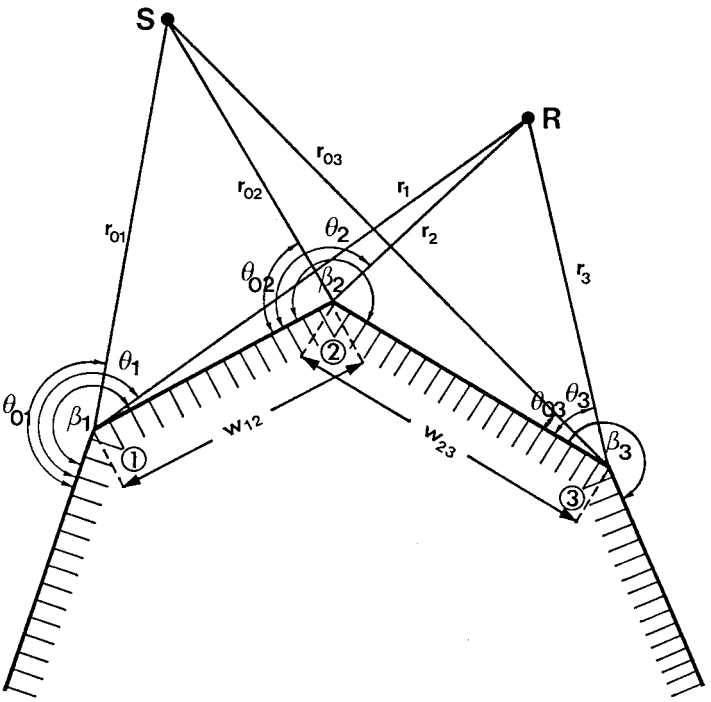

Fig. F1. Geometry of a three wedged barrier.

singly diffracted rays have the ability to touch upon other edges. Considering Fig. F1, one could develop the expression of the diffracted wave given by the GTD in the form (E1) in a new form which reads as [21]

$$u_d(\theta, r) = \frac{e^{ik(r_0+r)}}{r_0 + r}\left[V_d\left(\frac{r_0 r}{r_0 + r}, \theta - \theta_0\right) + V_d\left(\frac{r_0 r}{r_0 + r}, 2\beta + \theta + \theta_0\right)\right] \tag{F1}$$

with:

$$\begin{aligned} V_d(BA, \theta) &= V_{d+}(BA, \theta) + V_{d-}(BA\theta) \\ V_{d\pm}(BA, \theta) &= \frac{e^{i\pi/4}}{\sqrt{2\pi kl}}\frac{\beta}{2\pi}\cot\left(\frac{\pi \pm \theta}{2\pi/\beta}\right)F(BX_{\pm}\theta) \end{aligned} \tag{F2}$$

and here:

$$F(x) = -2i\sqrt{x}\, e^{-ix}\int_{\sqrt{x}}^{\infty} e^{i\tau^2} d\tau \tag{F3a}$$

$$X_{\pm}(\theta) = 2kA\cos^2\left(\frac{2N_{\pm}\beta - \theta}{2}\right) \tag{F3b}$$

$$N_+ = \begin{cases} 0 & \theta \leqslant \beta - \pi \\ 1 & \theta > \beta - \pi \end{cases} \quad N_- = \begin{cases} -1 & \theta < \pi - \beta \\ 0 & \pi - \beta \leqslant \theta \leqslant \pi + \beta \\ +1 & \theta > \pi + \beta \end{cases} \tag{F3c}$$

With these definitions, the double diffracted field [20] (by considering for example in Fig. F1 the wedges 1 and 2 a distance w_{12} apart) is given the new expression [21]:

$$\begin{aligned} u_{d12} &= 2\exp[ik(r_{01} + w_{12} + r_{\cdot 2})]/(r_{01} + w_{12} + r_2) \\ &\quad \cdot V_d\left[B(r_{01}, r_2, w_{12})\frac{r_{01}(w_{12} + r_2)}{(r_{01} + w_{12} + r_{12})}, \theta_{01}\right] V_d\left[\frac{(r_{01} + w_{12})r_2}{(r_{01} + w_{12} + r_2)}, \beta_2 - \theta_2\right] \\ &\quad \text{for } X_-(\theta_{01}) \leqslant X_-(\beta_2 - \theta_2) \\ &\quad \cdot V_d\left[\frac{r_{01}(w_{12} + r_2)}{(r_{01} + w_{12} + r_2)}, \theta_{01}\right] V_d\left[B(r_{01}, r_2, w_{12})\frac{(r_{01} + w_{12})r_2}{(r_{01} + w_{12} + r_2)}, \beta_2 - \theta_2\right] \\ &\quad \text{for } X_-(\theta_{01}) > X_-(\beta_2 - \theta_2) \end{aligned} \tag{F4}$$

where:

$$B(r_0, r, w) = w(w + r_0 + r)/(w + r_0)(w + r) \tag{F5}$$

This last expression is given under the conditions:

$$kr, kr_0, kw >> 1, k = (2\pi f/c) \tag{F6}$$

that is in the high frequency range where at any rate the assumptions of geometric optics should be satisfied.

Similary, by considering the wedges 1, 2 and 3, the possibility of a triple diffracted ray could not be avoided if one considers fro instance the previous double diffracted ray to get diffracted for instance the previous double diffracted ray to get diffracted at the wedge 3. The expression for this field is:

$$\begin{aligned} u_{d123} &= 2\exp[ik(r_{01} + w_{12} + w_{23} + r_3)]/(r_{01} + w_{12} + w_{23} + r_3) \\ &\quad \cdot V_d\left\{B(r_{01}, w_{23} + r_3, w_{12})\frac{r_{01}(w_{12} + w_{23} + r_3)}{r_{01} + w_{12} + w_{23} + r_3}, \theta_{01}\right\} \\ &\quad \cdot V_d\left\{B(r_{01}, w_{12} + r_3, w_{23})\frac{(r_{01} + w_{12})(w_{23} + r_3)}{r_{01} + w_{12} + w_{23} + r_3}, \beta_2\right\} \\ &\quad \cdot V_d\left\{\frac{(r_{01} + w_{12} + w_{23})r_3}{r_{01} + w_{12} + w_{23} + r_3}, \beta_3 - \theta_3\right\} \\ &\quad \text{for } |X_-(\theta_{01})| \leqslant |X_-(\beta_2)|, |X_-(\beta_2)| \leqslant |X_-(\beta_3 - \theta_3)| \end{aligned} \tag{F7}$$

and in case $|X_-(\theta_{01})| > |X_-(\beta_2)|$, $B(r_{01}, w_{23} + r_3, w_{12})$ is inserted into the secon V_d, while for $|X_-(\beta_2)| > |X_-(\beta_3 - \theta_3)|$, $B(r_{01} + w_{12}, r_3, w_{23})$ is inserted into the third V_d.

To apply these results to our problem of interest, the strip may be considered as the degeneration of a double wedge when its exterior angles extend to 2π. The angles sustaining the source or the field point rays can simply be decided from geometrical considerations in the drawings.

References

[1] Born M, Wolf E. Principles of optics. 6th ed. Oxford: Pergamon Press, 1986.
[2] Biot MA, Tolstoy I. Formulation of wave propagation in infinite media by normal coordinates with an application to diffraction. Journal of the Acoustical Society of America 1957;29:381–91.
[3] Medwin H. Shadowing by finite noise barriers. Journal of the Acoustical Society of America 1981;69:1060–4.
[4] Kinney WA, Clay CS, Sandness GA. Scattering from a corrugated surface: comparison between experiment, Helmholtz–Kirchhoff theory and the facet ensemble method. Journal of the Acoustical Society of America 1983;73:183–94.
[5] Gradshteyn IS, Ryzhik IM. Table of integrals, series and products (formula 17.33.3). Orlando: Academic Press, 1980. p. 1150
[6] Newland DE. An introduction to random vibrations and spectral analysis 2nd ed. New York: Longman, 1986.
[7] Roberts GE, Kaufman H. Table of laplace transforms (formula 2.1.3). W.B. Saunders Company, 1966, p. 16.
[8] NAG (The Numerical Algorithm Group), Mark 15, Oxford, 1985.
[9] Kravtsov Yu A, Rays and caustics as physical objects. In: Wolf E, editor. Progress in Optics vol. XXVI. Elsevier Science, 1988. p. 228–348.
[10] Ufimtsev PY. Theory of acoustical edge waves. Journal of the Acoustical Society of America 1989;86:463–74.
[11] Keller JB. The geometrical theory of diffraction. Journal of the Optical Society of America 1962;52:116–30.
[12] Sommerfeld A. Optics. Lectures in theoretical physics. New York: Academic Press.
[13] Kouyoumjian RG, Pathak PH. A uniform geometrical theory of diffraction for an edge in a perfectly conducting surface. Proceedings of IEEE 1974;62:1448–61.
[14] Garnir MG. Fonctions de Green de l'opérateur methaharmonique pour les problémes de Dirichlet et de Neumann posés dans un angle ou un diédre. Bulletin de la Société Royale de Liége 1952;21:207–31.
[15] Hadden WT, Pierce AD. Sound diffraction around screens and wedges for arbitrary point source locations. Journal of the Acoustical Society of America 1981;69:1266–76.
[16] Hadden WT, Pierce AD. Erratum to Ref. [15]. Journal of the Acoustical Society of America 1982;71:1290.
[17] Ambaud P, Bergassoli A. Le problem du diédre en acoustique. Acustica 1972;27:291–8.
[18] Papadopoulos AI, Don CG. A study of barrier attenuation by using acoustic impulses. Journal of the Acoustical Society of America 1991;90:1011–8.
[19] Grannemann WW, Watson RB. Diffraction of electromagnetic waves by a metallic wedge of acute dihedral angle. Journal of Applied Physics 1955;26:392–3.
[20] Pierce AD. Diffraction of sound around corners and over wide barriers. Journal of the Acoustical Society of America 1974;55:941–55.
[21] Kawai T. Sound diffraction by many sided barrier or pillar. Journal of Sound and Vibration 1981;79:229–42.
[22] Morimoto M, Maekawa Z. Effects of low frequency components on auditory spaciousness. Acustica 1988;66:190–6.

[23] Barron M, Marshall AH. Spatial impression due to early lateral reflections in concert halls: the derivation of a physical measure. Journal of Sound Vibration 1981;77:211–32.
[24] Blauert J. Binaural localization: multiple images and applications in room and electroacoustics. In: Shaw EAG, editor. Sound localization. Amphora Press, 1982 (chapter 5).
[25] Cremer L. Early lateral reflections in some modern concert halls. Journal of the Acoustical Society of America 1989;85:1213–25.
[26] Blauert J. Spatial hearing. Cambridge (MA): MIT Press, 1983.
[27] Cremer L, Müller HA, Schultz TJ. Principles and applications of room acoustics. London: Applied Science, 1982.
[28] Abramowitz M, Stegun I. Handbook of mathematical functions. New York: Dover Publications, 1972.
[29] Medwin H, Childs E, Jebsen GM. Impulse studies of double diffraction: a discrete Huygens interpretation. Journal of the Acoustical Society of America 1982;72:1005–13.